This is to certify that the

thesis entitled

EXPERIMENTAL INVESTIGATION OF CIRCULAR PATH CENTRIFUGAL PENDULUM VIBRATION ABSORBERS

presented by

TYLER MONROE NESTER

has been accepted towards fulfillment of the requirements for

M.S. degree in Mechanical Engineering

Major professor

Date 6/26/02

EXPERIMENTAL INVESTIGATION OF CIRCULAR PATH CENTRIFUGAL PENDULUM VIBRATION ABSORBERS

By

Tyler Monroe Nester

A THESIS

Submitted to
Michigan State University
in partial fulfillment of the requirements
for the degree of

MASTER OF SCIENCE

Department of Mechanical Engineering

2002

ABSTRACT

EXPERIMENTAL INVESTIGATION OF CIRCULAR PATH CENTRIFUGAL PENDULUM VIBRATION ABSORBERS

By

Tyler Monroe Nester

This work investigates various aspects of circular path centrifugal pendulum vibration absorbers (CPVA's). The main topics addressed in this thesis are: comparing the experimental and theoretical dynamics of one pendulum absorber attached to a rotating system, the dynamics of four pendulum absorbers attached to a rotating system, and documenting the performance improvements attained by installing CPVA's in a commercial internal combustion engine. Experimental results for the steady-state responses of the pendulum absorbers at various torque levels and excitation frequencies are presented. These responses are compared to approximate theoretical results and numerical simulations based on previous works. The well-known jump bifurcation is shown to exist in both the single absorber and the multi-absorber system. In the multi-absorber case, the bifurcation to a non-unison response is experimentally shown.

This work also examines experimental data obtained from measuring the vibration levels from an experimental vehicle with circular path CPVA's attached to the crankshaft. By comparing these results to measurements taken from a similar truck without absorbers, it is shown that the CPVA's successfully lowered the vibration levels in the vehicle at the desired excitation order.

To my wife and family

ACKNOWLEDGMENTS

Numerous people have given me invaluable support while I have been working on this thesis, especially my advisor, Dr. Steven W. Shaw, and Dr. Alan Haddow for allowing me to work with them on this project. I would especially like to thank Dr. Shaw for giving me the opportunity to continue my education and work under his guidance over the last two and a half years. I would like to sincerely thank both Dr. Brian Feeny and Dr. Clark Radcliffe for all of their assistance during my time at Michigan State University. In addition, I would like to thank John Brevick and Victor Borowski.

Special thanks to Ford Motor Company, the National Science Foundation, and Michigan State University for their support of my research.

Thanks also to Brian Olson, Polarit Apiwattanalunggarn, Pete Schmitz, Mark Berry, Yi Wu, and Dr. Choong-Ming Jung for all of their assistance.

My wife and family have provided me with endless support and encouragement throughout the course of my research, and I would like to thank them for everything they have done.

TABLE OF CONTENTS

LIST OF FIGURES

LIST OF TABLES

CHAPTER ONE

INTRODUCTION

Rotating systems that are subjected to torque loadings that vary as a function of the angle of rotation arise in numerous applications, including internal combustion engines, turbines, helicopter rotors, industrial fans, and rotary aircraft engines. In the case of internal combustion engines, the firing of the cylinders subjects the crankshaft to a torque load that is dependent on the angle of rotation, while for helicopter rotors aerodynamic loads on the blades cause fluctuating torque loads on the rotor, and in centrifugal fans the fluctuating loads can be caused when the fan blades pass the exit. For these systems, the fluctuating torque loads cause torsional vibrations that will be present at all operating speeds throughout the range of operation. Many of these systems can be modeled as being subjected to a constant mean torque, which keeps the system operating at a nominally constant speed Ω, and a fluctuating torque with a frequency n times that of the system's mean rotation speed. These types of torque loads are referred to as order n torques and result in torsional vibrations at a primary frequency of $n\,\Omega$. Centrifugal pendulum vibration absorbers (CPVA's) are ideally suited to eliminating this type of vibration, due to the fact that their natural frequency is a multiple of the rotation rate, that is, they can be tuned to a given order as opposed to a given frequency.

CPVA's were originally invented for use in internal combustion engines and were used as early as 1929 [1]. In addition to being used to reduce torsional vibrations in internal combustion engines, CPVA's have also been used to eliminate torsional vibrations in light aircraft engines [2, 3, 4], racing engines [5], and helicopter rotors [6].

A number of other previous works have focused on analyzing the optimum path for the absorber [7,8]. In addition to path considerations, previous works have analytically addressed the effects of nonlinearities and damping [9], the concept of localization in systems with nearly identical absorbers [10], and the stability of the unison response in systems with several nearly identical absorbers [11].

The primary focus of this work is the experimental investigation of circular path CPVA's in laboratory experiments and in internal combustion engines. The next section of this chapter discusses the operation of CPVA's in more detail. In section 1.2, previous work in this area is discussed in order to motivate the current study, and the organization of the remainder of this thesis is outlined in section 1.3.

1.1 Operation of CPVA's

The torsional vibrations caused by order n torque loadings can cause severe vibration problems. These vibrations can be potentially damaging to the rotating system itself and they can also be transmitted into the surrounding structures and the environment in the form of either noise or forces. These vibrations can render a product displeasing to consumers, and can even lead to premature fatigue failure of the rotating system or surrounding structures. Numerous methods, including the addition of inertia in the form of flywheels or lumped masses [12], the implementation of tuned vibration dampers [3, 13, 14], or the use of an active control system, can be used to reduce the vibration levels present in these systems. Each of these methods has drawbacks. In addition to increasing the mass of the system, the increased inertia of flywheels generally makes the system less responsive. Tuned vibration dampers are very efficient at eliminating particular frequencies of vibration, or in some cases specific but narrow ranges of frequencies, but they have limited effectiveness for eliminating torsional vibrations because they are only effective at a specific frequency. In the cases when a wide range of frequencies must be absorbed, such as in an internal combustion engine or a variable speed fan, a tuned vibration absorber would have to be used for each potential resonance frequency in the entire operating range. Even if there were a way to attach all of the required absorbers to the system, this approach would lead to excessive cost. In addition, torsional dampers dissipate energy and generate heat. Active control systems require sensors, actuators, control logic, and a power supply which makes the total cost of an active control system more than most, if not all, passive control solutions for these types of rotating systems.

Centrifugal pendulum vibration absorbers have numerous characteristics that make them more attractive than the methods listed above for controlling vibration problems caused by order n torques. CPVA's absorb vibrations at an order of the rotation rate, so they can be tuned to absorb order n torques throughout the range of operating rotation speeds. Additionally, CPVA's dissipate essentially zero energy and are often designed so that they do not increase the rotational inertia of the system to which they are attached.

Centrifugal pendulum vibration absorbers are masses that move in a prescribed path relative to the rotating system. For the purposes of this thesis, the specified path is circular, but work has been done on cycloidal, epicycloidal, subharmonic epicycloidal, and general paths as well [8, 15]. The circular path absorber system, using bifilar CPVA's, has been shown to be equivalent to the system in Figure 1.1 [11], where the absorbers are idealized as point masses riding along paths on the rotor.

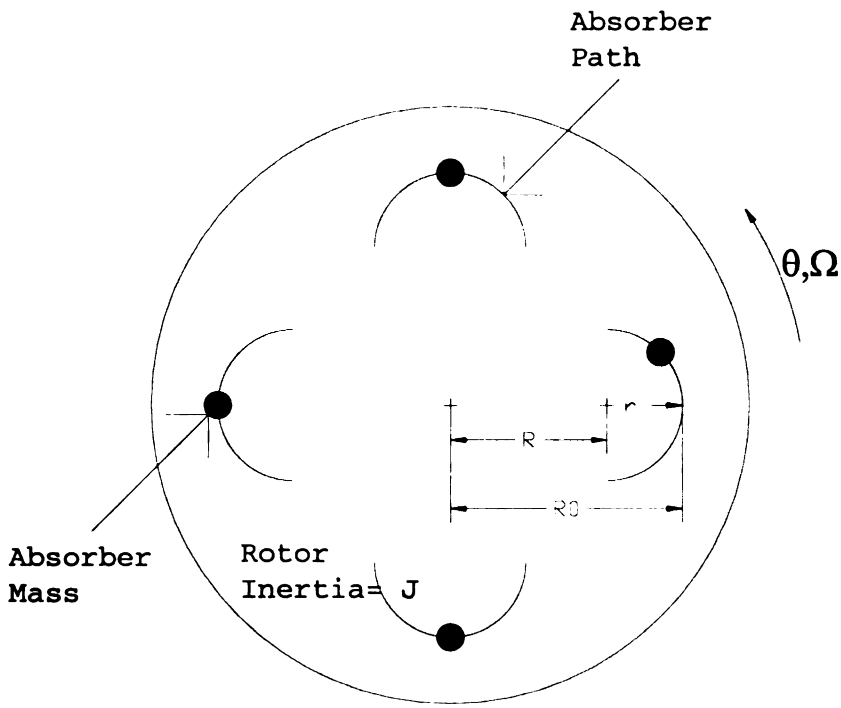

Figure 1.1: Rotor with four circular-path CPVA's.

The system of Figure 1.1 has been analyzed by Alsuwaiyan [11]. By choosing an appropriate scaling, the laboratory experiments reported in Chapter Three can be compared to the response of the system shown in Figure 1.1. According to linear theory, the order of the CPVA's in Figure 1.1 is given by:

$$n = \sqrt{\frac{R}{r}} \tag{1.1}$$

where R and r are the distances shown in Figure 1.1. By adjusting the radius of the absorber path and the absorber's center of rotation, it is possible to tune the CPVA to absorb any order of forcing. For constant rotor speed, Ω, the linearized natural frequency of the tuned absorber in Figure 1.1 is given by:

$$\omega = \Omega\sqrt{\frac{R}{r}} = n\Omega . \tag{1.2}$$

Equation 1.2 shows that the CPVA's natural frequency is a linear function of the rotation speed, which allows CPVA's to be used to absorb all the vibrations at order n over the entire operational range of rotor speeds. This property is what makes CPVA's preferable to traditional tuned vibration absorbers. Instead of eliminating one frequency and potentially making others worse, as is the case when using tuned vibration dampers, CPVA's make it possible to eliminate vibrations at a given multiple of the rotation rate.

1.2 History of CPVA's

The works by Ker Wilson [3], Den Hartog [16], and Chao [17] contain a detailed description of the history of centrifugal pendulum vibration absorbers. Much of the information included in this section is based on their descriptions. The following paragraphs present a brief history and some of the more recent developments in the theoretical understanding and applications of CPVA's.

According to Ker Wilson, Kutzbach achieved the earliest design incorporating a CPVA into a rotating system in 1911 when he proposed a mechanical arrangement that consisted of moving fluid in U-shaped channels mounted on the rotating system.

According to British Patent No. 337,466 Carter developed a roll-form absorber in 1929. In 1930, Meissner presented the results of experiments where he had used water columns in U-tubes to equalize the speed of rotating shafts. His results demonstrated the effectiveness of these devices and led to the development of numerous pendulum assemblies, which consisted mostly of solid pendulum masses, between 1930 and 1940. During this time, both bifilar pendulums and roll-form pendulum designs were developed which considered different path and damping parameters. In the United States, CPVA's were used to eliminate torsional vibrations in radial aircraft engines [2,12], and played a vital role in WWII aircraft development.

After the initial stages of developing various types of pendulum assemblies had been completed, tuning the pendulums and applying CPVA's became the focus of numerous research efforts. In 1934, the engine manufacturer Sulzer Brothers applied CPVA's to an in-line compression ignition engine. The Sulzer Brothers' manufactured numerous engine designs with absorbers that all operated problem-free for tens of thousands of hours without vibration problems. Numerous other engine manufacturers also achieved similar positive results with CPVA's during this time period [3].

More recently, CPVA's have seen application in the aerospace industry [18, 19] and in experimental automobile engines [20, 21, 22, 23]. In 1973, Wachs investigated the effects of CPVA's on helicopter reliability by monitoring the repair costs over a period of time for helicopters both with CPVA's and without CPVA's. He discovered that over a ten year time period the maintenance costs for helicopters retrofitted with CPVA's were an average of $367,311 less per aircraft than helicopters without CPVA's

[24]. Figure 1.2 shows an example of a helicopter rotor assembly with four roll-form CPVA's attached.

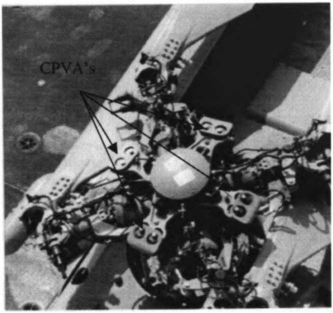

Figure 1.2: Helicopter rotor with CPVA's attached.

Although much work has been done in this area, past experimental work has been limited primarily to specific cases and applications. Specific engines, automobiles, and helicopters have been built and tested, but most previous experimental efforts have often been limited in scope to verifying that CPVA's lowered the vibration levels in the attached structure. No systematic, controlled experiments that monitored both the response of the absorbers and the rotor have been undertaken prior to this work.

1.3 Thesis Organization

The remainder of this thesis is organized as follows. Chapter Two addresses the theoretical background for circular path CPVA's while Chapter Three discusses the laboratory experiments performed. Specifically, many of these experiments focused on experimentally observing the behaviors first discovered by Alsuwaiyan [11] analytically and in simulations. The experimental setup used for the laboratory experiments, experiments with one absorber active, and experimental results with four absorbers active each all discussed in Chapter Three. In Chapter Three, systematic experiments are carried out at multiple excitation orders and torque levels. By performing experiments over a wide range of operating conditions, the behavior of CPVA's throughout their design space is illustrated.

Chapter Four discusses the vibration measurements obtained from an experimental vehicle with CPVA's attached to the crankshaft. These measurements are compared to baseline measurements that were obtained from a comparable vehicle without CPVA's. The final Chapter presents a discussion of these results, including a summary of the main contributions, and lists some recommendations for future work.

CHAPTER TWO

THEORETICAL BACKGROUND

2.1 Equations of Motion

The experiments reported in Chapter Three of this thesis primarily investigate experimental verification of the analytical results obtained by Alsuwaiyan and Shaw [10, 11]. Here we develop an analytical model for the experimental system, a schematic of which is shown in Figure 2.1. The distinction between the systems of Figure 1.1 and 2.1 is that the system shown in Figure 2.1 has absorbers which have non-zero moments of inertia about their centers of mass while the system shown in Figure 1.1 has point-mass absorbers.

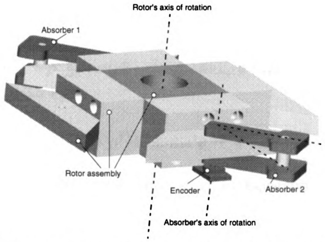

Figure 2.1: Schematic diagram of rotor with two T-shaped CPVA's attached.

The equations of motion for the system shown in Figure 2.1 with a single absorber were obtained using LaGrange's method. When the applied torque is an order n torque, the rotor angle is denoted by θ, and the absorber angle is denoted by ϕ, these equations are given by:

$$\begin{aligned}&\left[J+mR^2+m\left(r^2+\rho^2\right)+2mrR\cos\phi\right]\ddot{\theta}+m(rR\cos\phi+r^2+\rho^2)\ddot{\phi}\\&-mrR[2\dot{\theta}+\dot{\phi}]\dot{\phi}\sin\phi+c_0\dot{\theta}=T_0+T\sin(n\theta)\end{aligned} \tag{2.1}$$

$$m(rR\cos\phi+r^2+\rho^2)\ddot{\theta}+m\left(r^2+\rho^2\right)\ddot{\phi}+mrR\dot{\theta}^2\sin\phi+c_a\dot{\phi}=0 \tag{2.2}$$

where c_a and c_0 represent the absorber and rotor damping coefficients, respectively, m is the mass of the absorber, J is the rotor inertia, R is the distance from the rotor's center to the absorber's center of rotation, ρ is the absorber's radius of gyration about its center of mass, T_0 is the mean torque, T is the fluctuating torque amplitude, and r is the distance from the absorber's center of rotation to its center of mass.

For small absorber amplitudes, $|\phi|<<1$, and small deviations about a constant operating speed of Ω,

$$\theta=\Omega t+\psi,\ |\psi|<<1 \tag{2.3}$$

Equations 2.1 and 2.2 reduce to:

$$\begin{aligned}&\left[J+m\left((R+r)^2+\rho^2\right)\right]\ddot{\psi}+m(rR+r^2+\rho^2)\ddot{\phi}+c_0(\dot{\psi}+\Omega)\\&=T_0+T\sin(n(\Omega t+\psi))\end{aligned} \tag{2.4}$$

$$m(rR+r^2+\rho^2)\ddot{\psi}+m\left(r^2+\rho^2\right)\ddot{\phi}+mrR\Omega^2\phi+c_a\dot{\phi}=0 \tag{2.5}$$

Den Hartog analyzed the linearized system given by Equations 2.4 and 2.5 with $\rho=0$, $c_a=0$, $c_0=0$, and $T_0=0$, and showed that the identically tuned pendulum corresponds to a system with an infinite amount of positive rotor inertia while an undertuned pendulum and overtuned pendulum correspond with a negative and a large inertia, respectively [16].

For a constant rotor speed ($\dot{\theta}$=Ω=const.), it is clear that the pendulum's undamped natural frequency is given by:

$$\omega_0 = \Omega\sqrt{\frac{rR}{\left(r^2+\rho^2\right)}} \tag{2.6}$$

Equivalently, the pendulum tuning order can be expressed as:

$$\tilde{n} = \sqrt{\frac{rR}{\left(r^2+\rho^2\right)}} \tag{2.7}$$

(which reduces to $\sqrt{R/r}$ for a point mass, ρ=0). For a system with an order n torque, a CPVA is referred to as being overtuned (undertuned) when $\tilde{n}>(<)n$. Absorbers are generally overtuned, for reasons described subsequently.

As the applied fluctuating torque amplitude increases, the absorber amplitude increases until it reaches a critical point at which the amplitude jumps, which is a consequence of a saddle node bifurcation. This behavior results from the fact that the frequency of oscillation of a circular path pendulum is dependent on the amplitude of oscillation. This phenomenon was investigated by Newland [4]. He observed that absorber swing angles above 25° could cause a nonlinear jump in the absorber amplitude, which was accompanied by a 180° change in the absorber's phase angle [4]. This change in the phase angle after the jump in the absorber's response amplitude causes the absorber to amplify the applied torque rather than absorb it. Similarly, as the amount of absorber overtuning is increased, the torque amplitude required to cause a jump also increases, thereby extending its operating range. This behavior, which will be shown both experimentally and numerically, emphatically demonstrates that nonlinear effects cannot be ignored. In order to design the CPVA so that it will be in tune for a given absorber amplitude, Newland proposed a set of detuning guidelines for point-mass or bifilar absorbers [4]. The guidelines given below were developed by generalizing Newland's results for absorbers with a non-zero radius of gyration about their center of mass and are given by:

$$\frac{rR}{\left(r^2+\rho^2\right)} = n^2(1+\varepsilon)$$
$$(1+\varepsilon) = \frac{\Phi_0}{2J}. \tag{2.8}$$

These define the way that r, ρ, and R must combine in order for the CPVA to be in tune at a specified absorber amplitude, Φ_0, for an order n torque. By following the guidelines given by Equation 2.8, the pendulums behave like overtuned absorbers according to Equation 2.7 for small amplitudes and then as the absorber amplitude increases, the absorber comes into a tuned condition [4].

In practice, circular path absorbers are always overtuned to avoid the potentially dangerous nonlinear jumps that occur at low torques in the perfect tuning case. This procedure has been used effectively in light aircraft engines, helicopter rotors, and experimental internal combustion engines [18, 20, 21, 23, 24].

2.2 Scaling Analysis

In order to compare the experimental results presented in Chapter Three with theoretical and numerical predictions of Alsuwaiyan and others, Equations 2.1 and 2.2 must be rescaled so that they match the form of the equations used by previous researchers [8, 10, 11, 17, 25]. The first step in this conversion is to express the absorber position in Equations 2.1 and 2.2 in terms of a non-dimensional arc length given by:

$$s = \frac{r\phi}{\beta} \tag{2.10}$$

where β will be selected later to obtain the desired form of the rescaled equations. Substituting Equation 2.10 into Equations 2.1 and 2.2 yields:

$$\begin{gathered}\left[J + mR^2 + m\left(r^2+\rho^2\right) + 2mrR\cos\left[\frac{\beta s}{r}\right]\right]\ddot{\theta} + mrR\left(\cos\left[\frac{\beta s}{r}\right] + r^2 + \rho^2\right)\left[\frac{\beta \ddot{s}}{r}\right] \\ - mR\left[2\dot{\theta} + \frac{\beta \dot{s}}{r}\right]\left(\beta \dot{s}\right)\sin\left[\frac{\beta s}{r}\right] + c_0\dot{\theta} = T\sin(n\theta)\end{gathered}, \tag{2.11}$$

$$m\left(rR\cos\left[\frac{\beta s}{r}\right] + r^2 + \rho^2\right)\ddot{\theta} + m\left(r^2+\rho^2\right)\left(\frac{\beta \ddot{s}}{r}\right) + mrR\dot{\theta}^2\sin\left[\frac{\beta s}{r}\right] + c_a\dot{\theta} = 0. \tag{2.12}$$

These equations represent an autonomous dynamical system in s and θ because the forcing term depends on the rotor angle θ. For subsequent analysis, the system needs to be transformed so that the independent variable is the rotor angle, replacing time. To accomplish this, a new non-dimensional rotor speed variable, v, is defined as:

$$v \equiv \frac{\dot{\theta}}{\Omega} \tag{2.13}$$

where Ω is the mean rotor speed. Assuming $0<\varepsilon\ll 1$ and expanding the rotor speed, Alsuwaiyan [11] obtained the following expression that relates the rotor speed to the scaling:

$$v(\theta) = 1 + \varepsilon^{\frac{3}{2}}v_1(\theta) + H.O.T. \tag{2.14}$$

which is used to obtain the correct form for the angular acceleration of the rotor. ε will be defined below. Using the chain rule, it is possible to obtain the following relationships between derivatives with respect to time and derivatives with respect to θ:

$$\begin{aligned} (\dot{*}) &= \frac{d(*)}{dt} = \Omega v \frac{d(*)}{d\theta} = \Omega v (*)' \\ (\ddot{*}) &= \frac{d^2(*)}{dt^2} = \Omega^2 v \frac{dv}{d\theta}\frac{d(*)}{d\theta} + \Omega^2 v^2 \frac{d^2(*)}{d\theta^2} = \Omega^2 v v'(*)' + \Omega^2 v^2 (*)'' \end{aligned} \tag{2.15}$$

with the special important case of:

$$\ddot{\theta} = \frac{d^2\theta}{dt^2} = \Omega^2 v \frac{dv}{d\theta} = \Omega^2 v v' \ . \tag{2.16}$$

Substituting the above results into Equations 2.11 and 2.12, expanding sines and cosines to third order in s, and simplifying the results yields:

$$\begin{aligned} &\left[1 + m(r^2+\rho^2+R^2) + \frac{2mrR}{J} - \frac{mrR}{J}\left(\frac{\beta^2}{r^2}\right)s^2\right] v v' \\ &+ \left[\varepsilon - \frac{m\beta^3 R}{2Jr^2}s^3\right](vv's' + v^2 s'') - 2mR\beta(vs')^2\left(s - \frac{\beta^2}{6r^2}s^3\right) + O(s^4) = \Gamma_\theta(\theta) \end{aligned} \tag{2.17}$$

$$\begin{aligned} &v's' + vs'' + \left[\frac{r^2 R}{\beta(r^2+\rho^2)}\left(1 - \frac{1}{2}\left(\frac{\beta s}{r}\right)^2\right) + \frac{r}{\beta}\right] v' \\ &+ \frac{rR}{(r^2+\rho^2)}\left(s - \frac{\beta^2}{6r^2}s^3\right) v + \mu_a s' + O(s^4) = 0 \end{aligned} \tag{2.18}$$

where the following definitions have been made:

$$\begin{aligned} \varepsilon &\equiv \frac{m\beta}{Jr}\left(rR + r^2 + \rho^2\right) \\ \Gamma_\theta(\theta) &\equiv \frac{T\sin(n\theta)}{J\Omega^2} \\ \mu_a &\equiv \frac{c_a}{\Omega m(r^2+\rho^2)} . \end{aligned} \tag{2.19}$$

ε represents a particular ratio of absorber inertia to rotor inertia and is the "small" parameter that will be used to apply the method of averaging to Equations 2.17 and 2.18. It is selected so that the expanded equations match previous analytical works. μ_a represents the absorber damping, and Γ_θ is the non-dimensional fluctuating torque amplitude.

The nondimensional form of the equations of motion used by past researchers [10, 11, 25] for the unison response case for N identical absorbers is:

$$\begin{gathered}
vs''+\left[s'+\tilde{g}(s)\right]v'-\frac{1}{2}\frac{dx}{ds}(s)v=-\mu_a s' \\
\frac{NmR_0^2}{J}\left[\frac{dx}{ds}s'v^2+x(s)vv'+\tilde{g}(s)s'vv'+\tilde{g}(s)s''v^2+\frac{d\tilde{g}}{ds}(s)s^2v^2\right]+vv'= \\
\frac{NmR_0^2}{J}\mu_a\tilde{g}(s)s'v-\mu_0 v+\Gamma_0+\Gamma_\theta(\theta)
\end{gathered} \tag{2.20}$$

where μ_a is the absorber, the $x(s)$ is a normalized path function (defined below), Γ_0 and μ_0 refer to the mean torque and the rotor damping, respectively, and $\tilde{g}(s)$ is a path function arising from the Lagrangian derivation of the equations of motion. Expanding in terms of s, Alsuwaiyan [11] and Chao [17] showed that the form of $x(s)$ and $\tilde{g}(s)$ for a general absorber path are given by:

$$\begin{gathered}
x(s)=1-\tilde{n}^2 s^2+\gamma s^4+O(s^6),\text{ where} \\
\gamma(s)=\left(\frac{1}{12}\left(\tilde{n}^2+1\right)^2\left(\tilde{n}^2-\lambda^2\left(\tilde{n}^2+1\right)\right)\right),\text{ and} \\
\tilde{g}(s)=\sqrt{x(s)-\frac{1}{4}\left(\frac{dx}{ds}(s)\right)^2}=1-\frac{1}{2}\tilde{n}^2\left(1+\tilde{n}^2\right)s^2+O(s^4).
\end{gathered} \tag{2.21}$$

For circular paths, the case considered here, λ=0.

Observing that the mean torque and the rotor damping in Equation 2.20 must cancel each other ($\Gamma_0=\mu_0 \nu$), it is possible to match terms in Equation 2.20 to the corresponding terms in Equations 2.17 and 2.18. After matching terms, we obtain:

$$\tilde{g}(s)=\frac{r^2 R}{\beta\left(r^2+\rho^2\right)}\left(1-\frac{1}{2}\left(\frac{\beta^2}{r^2}\right)s^2\right)+\frac{r}{\beta}+O\left(s^4\right). \tag{2.22}$$

By choosing β we can force $\tilde{g}(s)$ to have the same form as given in Equation 2.21. Enforcing this condition yields:

$$\beta=r\left(1+\tilde{n}^2\right). \tag{2.23}$$

Continuing to match terms in Equations 2.17 and 2.18 with the corresponding terms in Equation 2.20, we obtain:

$$\frac{dx}{ds}=-2\tilde{n}^2\left(s-\frac{\beta^2}{6r^2}s^3\right)+O\left(s^5\right). \tag{2.24}$$

Integrating Equation 2.24, we obtain the following expression for the path function for the absorbers:

$$x(s)=C_1-\tilde{n}^2 s^2+\frac{\tilde{n}^2\left(1+\tilde{n}^2\right)}{12}s^4+O\left(s^6\right). \tag{2.25}$$

By choosing C_1=1 in Equation 2.25, the path function for the circular path absorbers in Equations 2.17 and 2.18 becomes:

$$x(s)=1-\tilde{n}^2 s^2+\gamma_0 s^4+O\left(s^6\right),\text{ with } \gamma=\frac{1}{12}\left(\tilde{n}^2+1\right)\tilde{n}^2. \tag{2.26}$$

Equation 2.26 shows that by choosing β and C_1 appropriately, Equations 2.17 and 2.18 can be scaled such that they have the same form as the Equations of motion investigated by previous researchers. This result allows us to follow their theoretical developments and compare our experimental results to their quite extensive theoretical and numerical results.

2.3 Averaged Equations and Synchronous Response

Alsuwaiyan [11] chose a scaling ε that allowed one to uncouple the absorber dynamics from the rotor dynamics. The scaling used was:

$$
\begin{aligned}
s &= \varepsilon^{\frac{1}{2}} z \\
\mu_a &= \varepsilon \tilde{\mu}_a \\
\Gamma_\theta &= \varepsilon^{\frac{3}{2}} \tilde{\Gamma}_\theta \\
\tilde{n} &= n(1+\varepsilon\sigma)
\end{aligned}
\tag{2.27}
$$

where σ is defined as a detuning parameter between the absorber tuning and the torque order and z represents the non-dimensional arc length displacement for the absorber normalized by β and $\varepsilon^{1/2}$. Substituting the above results into Equations 2.17 and 2.18 and keeping terms to order ε, we obtain the following Equation for the dynamics of the absorber:

$$
z'' + n^2 z = \varepsilon[2\gamma_0 z^3 - 2n^2 \sigma z - \tilde{\mu}_a z' - n^2 z - \tilde{\Gamma}_\theta \sin(n\theta)] + H.O.T. \tag{2.28}
$$

where γ_0 is given by:

$$
\gamma_0 = \frac{1}{12}\left(n^2+1\right)^2 n^2 \tag{2.29}
$$

for circular paths. Using Equation 2.28 in Equation 2.17, it is possible to obtain an expression for the angular acceleration of the rotor, which is a useful measure of the torsional vibrations. It is given by:

$$vv' = \varepsilon^{\frac{3}{2}}\left[n^2 z - \tilde{\Gamma}_\theta \sin(n\theta)\right] + H.O.T. \tag{2.30}$$

Once the absorber response has been determined using Equation 2.28, Equation 2.30 allows one to determine the rotor response.

The method of averaging was applied to Equation 2.28 to determine the approximate steady-state absorber amplitude for the synchronous response case as a function of the system parameters and the applied torque. In order to analyze Equation 2.28 using the method of averaging, the following transformation to polar coordinates is used:

$$\begin{aligned} z &= a\sin(n\theta + \phi) \\ z' &= na\cos(n\theta + \phi). \end{aligned} \tag{2.31}$$

By substituting Equation 2.31 into Equations 2.28 and averaging over one period of motion ($2\pi/n$), the following averaged equations that govern the averaged amplitude ($\bar{a}$) and phase ($\bar{\phi}$) of the absorber response can be obtained:

$$\begin{aligned} \bar{a}' &= \varepsilon\left[-\frac{\tilde{\mu}_a}{2}\bar{a} + \frac{\tilde{\Gamma}_\theta}{2n}\sin(\bar{\phi})\right] + H.O.T. \\ \overline{a\phi}' &= \varepsilon\left[-\frac{3\gamma_0}{4n}\bar{a}^3 + n\left(\sigma + \frac{1}{2N}\right)\bar{a} + \frac{\tilde{\Gamma}_\theta}{2n}\cos(\bar{\phi}) + \frac{n}{2}\bar{a}\right] + H.O.T. \end{aligned} \tag{2.32}$$

For steady-state conditions, $\bar{a} = r_z$ = constant, $\bar{\phi} = \phi_z$ = constant, which results in:

$$
\begin{aligned}
&\frac{\tilde{\mu}_a}{2} r_z = \frac{\tilde{\Gamma}_\theta}{2n}\sin(\phi_z) \\
&\frac{3\gamma_0}{4n} r_z^3 - n\left(\sigma + \frac{1}{2}\right) r_z = \frac{\tilde{\Gamma}_\theta}{2n}\cos(\phi_z).
\end{aligned}
\tag{2.33}
$$

Eliminating ϕ_z from Equation 2.33, the torque amplitude, Γ_θ, can be solved for in terms of the absorber amplitude and the system parameters for the unison absorber response case, yielding:

$$
\tilde{\Gamma}_\theta = 2n\sqrt{\left[\left(\frac{\tilde{\mu}_a}{2} r_z\right)^2 + \left(\frac{3\gamma_0}{4n} r_z^3 - n\left(\sigma + \frac{1}{2}\right) r_z\right)^2\right]}. \tag{2.34}
$$

Using Equation 2.34 it is possible to examine the response of the absorbers as a function of system and input parameters. The rotor's response is then found using Equation 2.30.

Figures 2.2-2.6 illustrate how various parameters affect the behavior of the rotor and the CPVA's. Specifically, Figure 2.1 shows that the lower nose of the absorber amplitude response curve shifts to the right as the level of detuning increases. This point corresponds to the location of the jump bifurcation. So, as level of detuning is increased, a larger torque excitation is required to cause a jump in the absorber's steady-state amplitude. For practical purposes, this means that an absorber is effective over a wider range of torque amplitudes for a larger level of mistuning. This increase is range is "paid for" by a corresponding increase in the rotor torsional vibrations, as shown below. Alsuwaiyan [11] showed that the analytical expression for the absorber amplitude at the jump bifurcation for the unison absorber response case is given by:

$$r_j \approx \frac{2n}{3}\sqrt{\frac{\left(\sigma+\frac{1}{2}\right)}{\gamma_0}}. \tag{2.35}$$

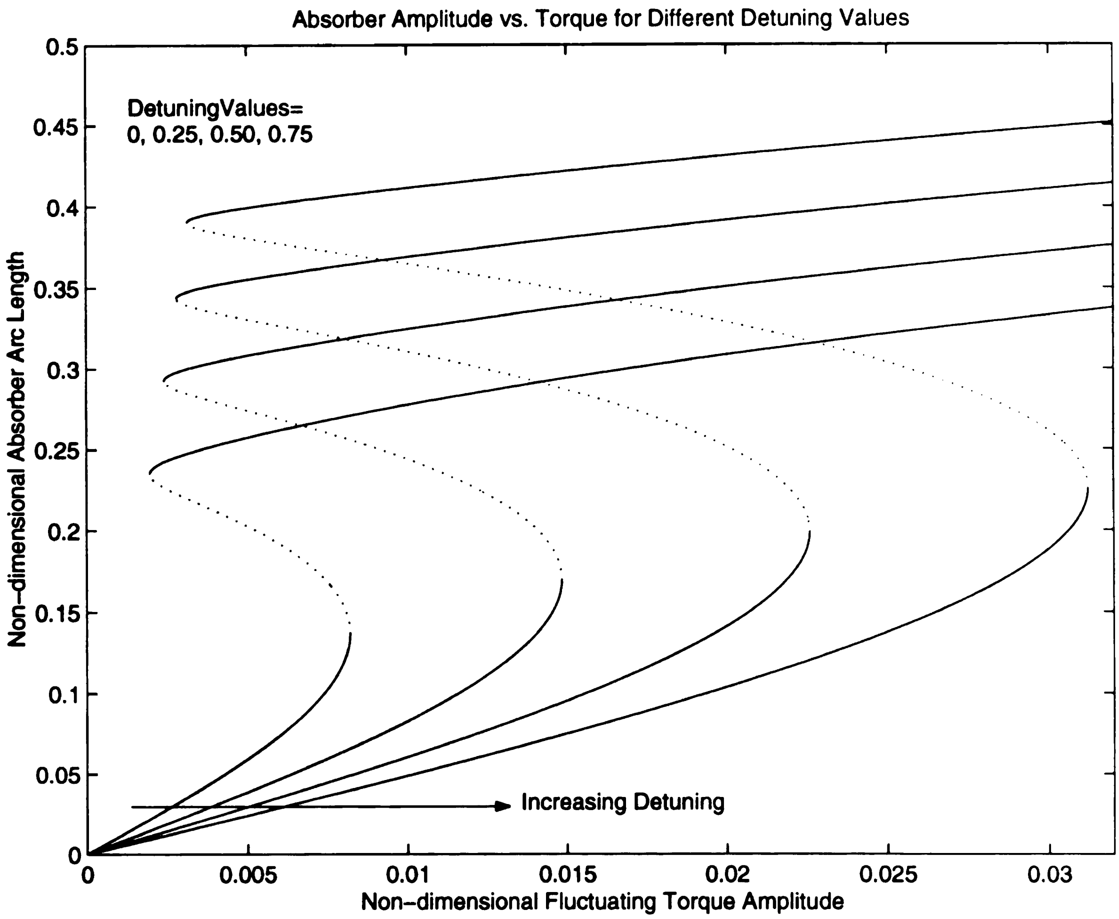

Figure 2.2: Absorber amplitude versus non-dimensional fluctuating torque amplitude for different levels of detuning with μ_a=0.00634.

In Figure 2.2, solid lines correspond to stable solutions, and dotted lines correspond to unstable solutions. Qualitatively, as the fluctuating torque amplitude is increased, the absorber amplitude increases until it reaches a critical value. At this critical value, increasing the torque amplitude causes the absorber response to turn back and become unstable, which results in a jump to the upper solution branch. This behavior is referred to as a jump and results from a saddle-node bifurcation. Conversely, when the absorber's response solution is on the upper branch, the response will stay on the upper branch as the torque amplitude is decreased until the jump bifurcation on the upper branch is encountered. This overall behavior is called hysteresis.

For purposes of practical applications, this means that once an absorber's amplitude has jumped to the upper branch, reducing the torque level to the previous level that corresponded to a solution on the lower branch of the absorber response curve is not sufficient to ensure that the absorber's response will return to the lower branch of the solution curve. The torque amplitude must be decreased until the absorbers reach the location of the jump bifurcation on the upper branch of the solution curve and jump back down to the lower branch of the solution curve. The amount of absorber mistuning determines the range of the effectiveness of the absorbers. The jump that occurs in Figure 2.2 is of great interest, because it can be shown that when the CPVA's are on the upper response curve, they actually amplify torsional vibrations.

By using Equations 2.30 and 2.34, it is possible to examine the rotor's angular acceleration, and by extension the torsional vibrations, as a function of system and input parameters. Figures 2.2 and 2.3 show how the level of absorber mistuning affects the angular acceleration of the rotor as the torque level is varied. In both Figure 2.2 and Figure 2.3, all of the factors except the amount of absorber mistuning are held constant. The results are compared to a rotor with the absorbers locked, which eliminates the flywheel effect that is caused by adding inertia to the system in the form of absorbers. This allows the system with absorbers to be compared to a system with the same amount of inertia, but no active absorbers. The straight line in Figure 2.3 shows the angular acceleration of the rotor when all of the attached absorbers are locked.

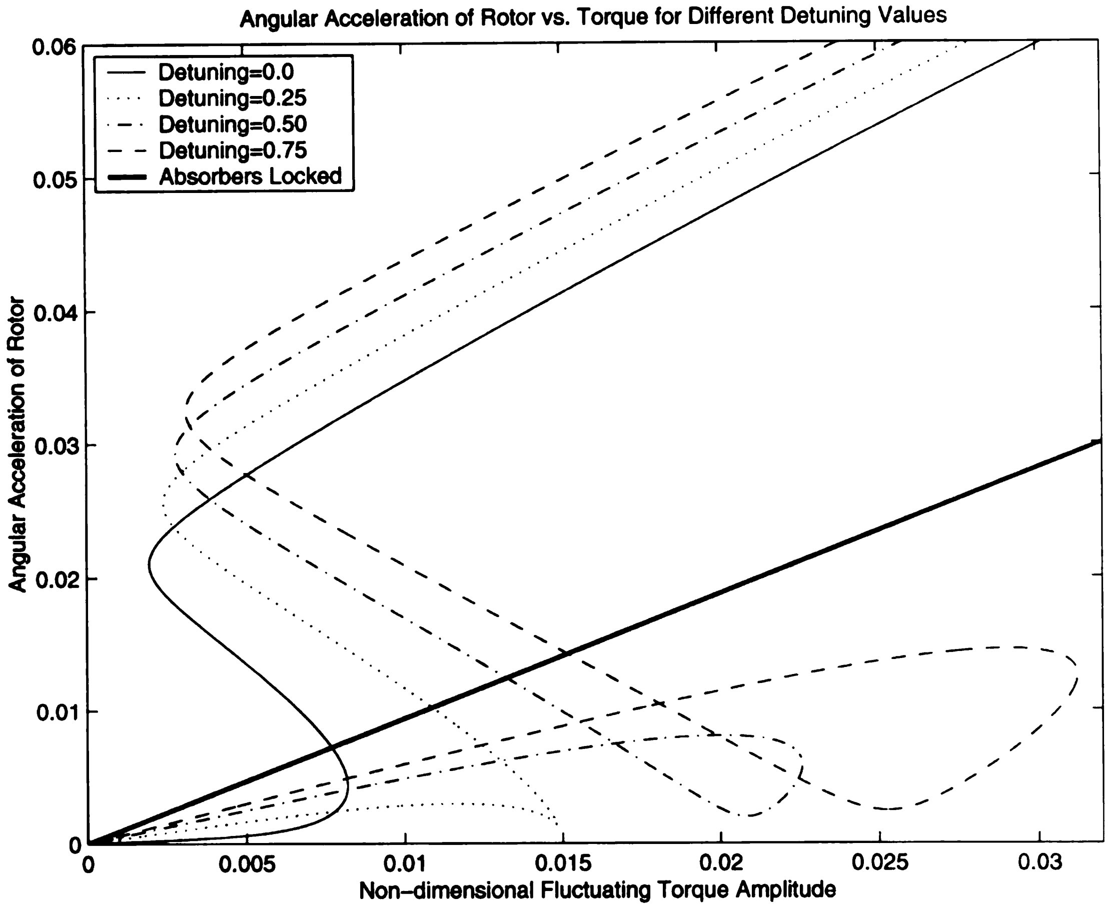

Figure 2.3: Angular acceleration of the rotor versus the fluctuating torque amplitude for the unison absorber response case for various levels of absorber mistuning.

For the ranges of mistuning shown, the rotor's angular acceleration is reduced compared to the case of locked absorbers, at least up to the jump point. However, Figures 2.2 and 2.3 indicate that CPVA's with lower levels of mistuning will go through the jump bifurcation at a lower torque amplitude than absorbers with higher levels of mistuning. Figure 2.3 also demonstrates that systems with CPVA's with small levels of mistuning offer better performance in terms of angular acceleration of the rotor, than systems with higher levels of mistuning. However, the cost of this improved performance is reduced operational range. In fact, the lowest angular acceleration is provided by perfectly tuned absorbers, but over a very limited torque range.

In addition to viewing the angular acceleration data as shown in Figure 2.3, it is also useful to look at the data normalized by the fluctuating torque amplitude, as shown in Figure 2.4. Figure 2.4 gives an indication of the amplification of the applied torque that occurs in the systems with pendulums with different levels of mistuning.

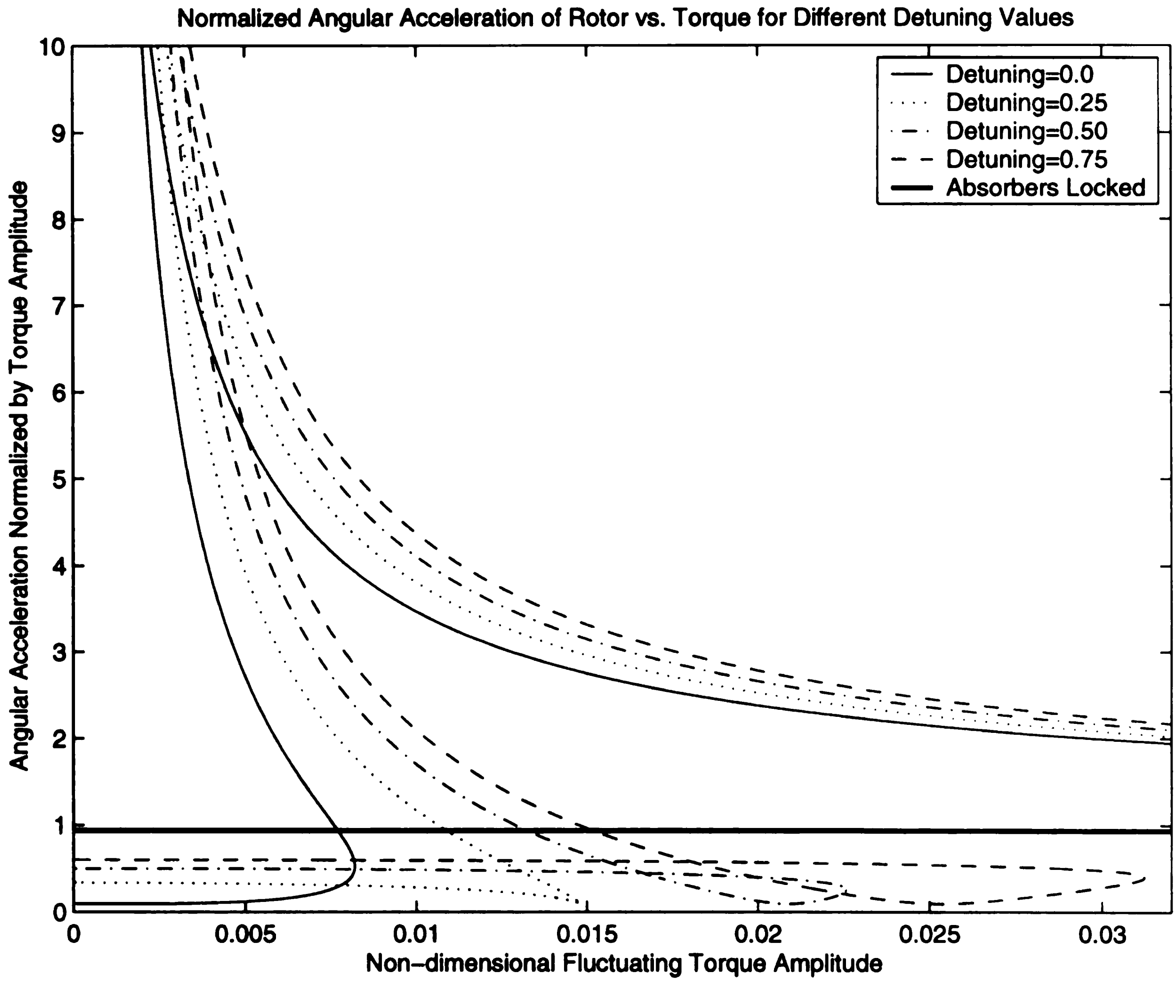

Figure 2.4: Angular acceleration of rotor normalized by the fluctuating torque amplitude versus the fluctuating torque amplitude for the unison absorber response case and various levels of absorber mistuning.

Figure 2.4, like Figure 2.3, shows that the absorbers lower the rotor's angular acceleration until they pass through the jump bifurcation. Additionally, the improved performance and reduced operating range for absorbers with lower mistuning are also illustrated here. In Figures 2.2-2.4, positive detuning values correspond to overtuned absorbers, negative values correspond to undertuned absorbers, and a detuning value equal to zero corresponds with a perfectly tuned absorber.

By holding the mistuning constant and varying the level of absorber damping, it is possible to obtain a qualitative picture of how the absorber damping affects the response. Figures 2.5, 2.6, and 2.7 show similar results for absorbers with different damping levels.

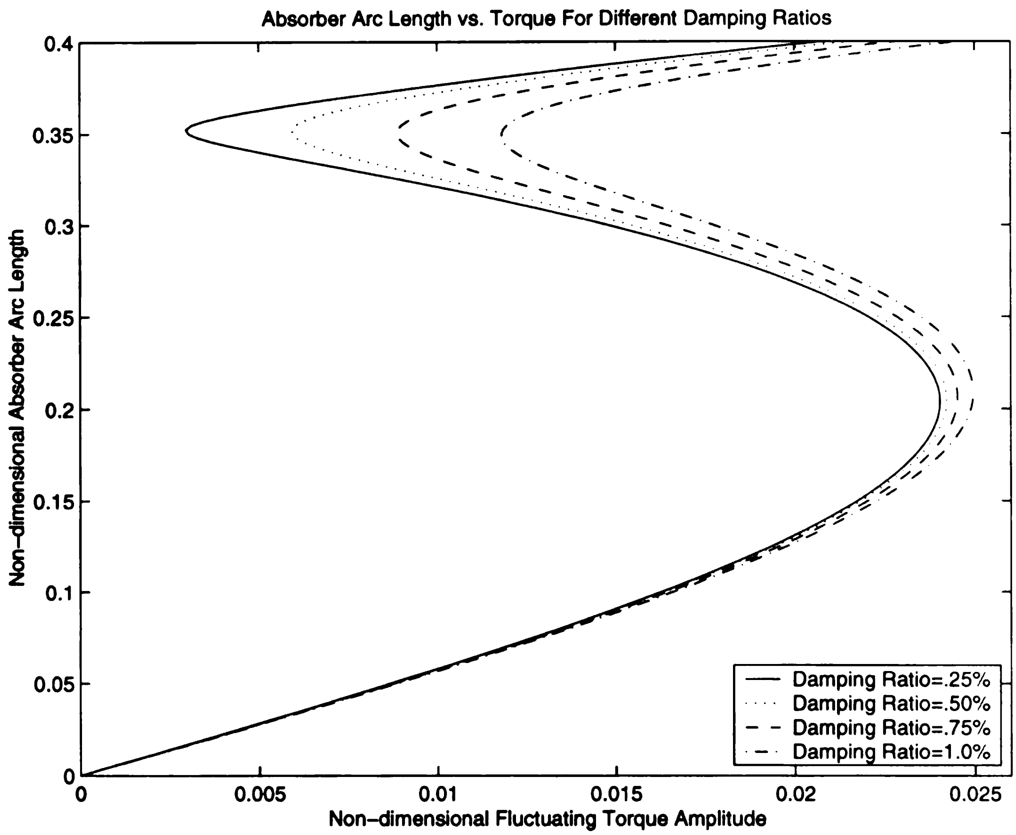

Figure 2.5: Steady-state absorber amplitude plotted versus the non-dimensional fluctuating torque amplitude.

Figure 2.5 illustrates that the behavior of the CPVA's is not altered significantly at low torque amplitudes on the lower branch by changing the damping ratio, but the location of the jump point on the upper branch of the solution curve is shifted to the right as the damping increases. For very lightly damped systems, the fluctuating torque amplitude will have to be decreased almost to zero, once the absorber's response has jumped, in order for the absorber's response to jump back down to the lower branch of the solution curve. This behavior enforces the theory that it is vital to the system's performance to ensure that the absorbers do not jump, because once they do, the system will essentially have to be shut down in order to return the absorbers to their intended mode of operation. For the same levels of absorber damping shown in Figure 2.5, Figure 2.6 shows how the angular acceleration of the rotor varies with increasing applied torque for different levels of absorber damping.

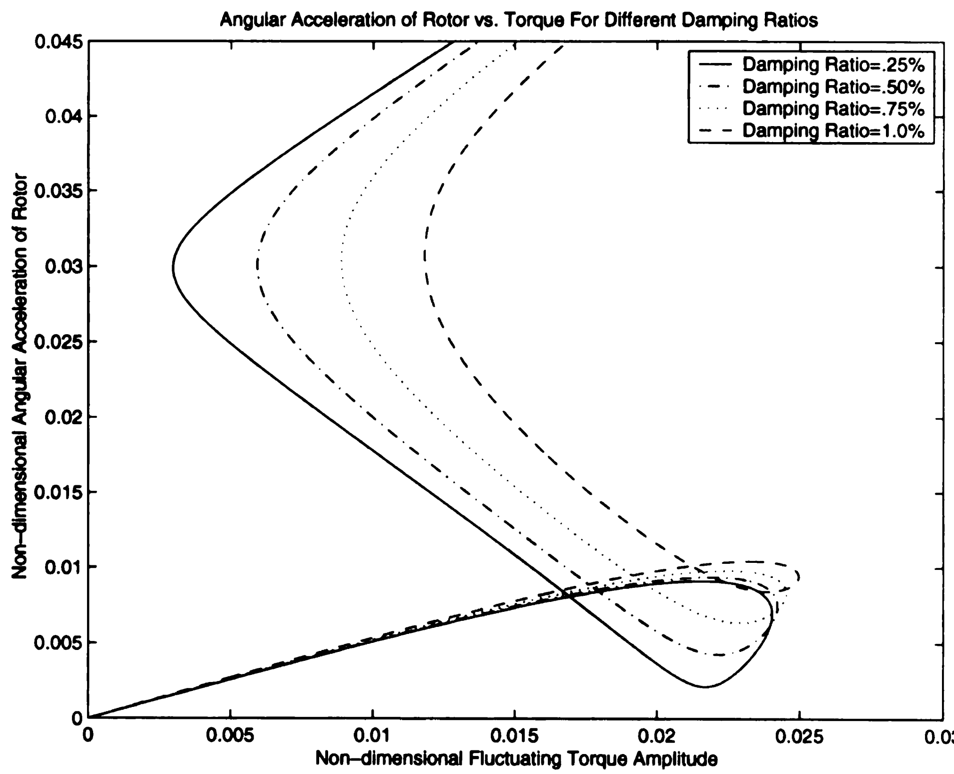

Figure 2.6: Steady-state angular acceleration of rotor plotted versus the fluctuating torque amplitude for different absorber damping ratios.

Figure 2.6 illustrates that the damping ratio does not have a large effect on the desired range of decreased angular acceleration.

In addition to considering how the amount of absorber damping affects the shape of the absorber response curve and the angular acceleration curve, it is also possible to investigate how this damping affects the relationship between the torque level at the maximum allowable absorber response angle and the absorber's level of mistuning. For Figure 2.7, the maximum allowable response angle was chosen to be the limiting angle that the experimental absorbers could swing through without hitting the rotor. Figure 2.7 shows the relationship between the fluctuating torque amplitude and the absorbers' mistuning level at the maximum response angle for different levels of damping.

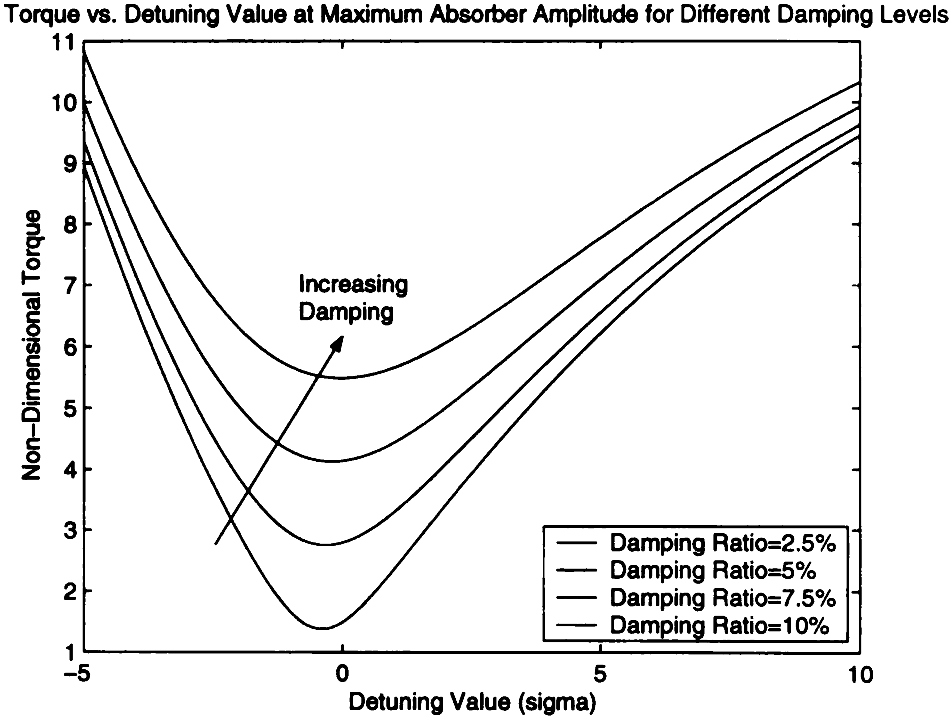

Figure 2.7: Non-dimensional fluctuating torque amplitude plotted versus detuning at the maximum absorber response and various damping levels.

Figure 2.7 illustrates that lightly damped absorbers will reach their maximum response for much lower torque levels than highly damped absorbers, especially near perfect tuning. These curves show the allowable torque amplitude at a given level of absorber mistuning.

2.4 Bifurcation to Non-Unison

In addition to the jump bifurcation in the unison absorber response, a bifurcation to non-unison responses exists for systems with multiple identical or nearly identical circular path absorbers. This bifurcation results in a loss of symmetry in the absorbers' responses. Alsuwaiyan showed that multiple groups of various response types exist after the system passes through this bifurcation. For example, after passing through this bifurcation, one absorber can oscillate while the remaining absorbers are inactive. The absorber amplitude at which the bifurcation to a non-unison response occurs is given by:

$$r_{NU} \approx \frac{4n}{\sqrt{54\gamma_0}}\left[3\sigma - \left((3\sigma)^2 - \frac{27}{4n^2}\left(n^2\sigma^2 + \frac{\bar{\mu}_a^2}{4}\right)\right)^{\frac{1}{2}}\right]^{\frac{1}{2}}. \tag{2.34}$$

Alsuwaiyan showed that absorbers can become localized as the torque level is increased and the system passes through the bifurcation to a non-unison response. When this occurs, a subset of absorbers have significantly larger response amplitude than the remaining absorbers. The severity of the localization was shown to be very sensitive to the mistuning differences between absorbers and the damping levels [11]. It was also shown for circular paths that the bifurcation to non-unison occurs at lower torque levels than the jump bifurcation. This result ensures that nonunison responses will be observed experimentally as the torque level varies, and at torque levels lower than the jump values.

Both the bifurcation to non-unison and the jump bifurcation will be shown in the experimental results in Chapter Three.

CHAPTER THREE

EXPERIMENTAL RESULTS

The main focus of this chapter is to present the experimental results performed on circular path CPVA's and compare these results to the simulation results and theoretical results obtained by previous researchers [10, 11]. The experimental apparatus, described in section 3.1, is instrumented such that the response of the CPVA's, the angular acceleration of the rotor, and the applied torque can all be accurately measured. Section 3.2 describes the procedures used to identify the various physical parameters that are needed in order to compare the experimental results to theoretical and numerical results. The experimental results for one absorber presented in section 3.3 were obtained by slowly increasing the fluctuating torque amplitude at a constant torque order and measuring the conditions at the resulting steady-state. The experimental results possess the key characteristics described in Chapter Two, where the theoretical background was developed for the T-shaped absorbers used in these experiments, which have a non-zero moment of inertia about their center of gravity. The experimental results in section 3.3 are compared to the theoretical curves developed in Chapter Two and numerical solutions based on the scaling developed in Chapter Two. Some observations about the behavior of systems with four absorbers are made in section 3.4, which demonstrates general features of the non-unison behavior of multi-absorber systems. A brief summary of the experimental results is presented in section 3.5.

3.1 Experimental Setup

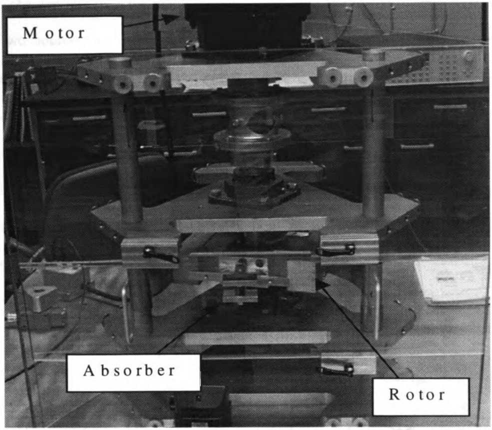

Figure 3.1: Photograph of rotor experimental frame, rotor assembly, and absorbers.

The experimental assembly used in these experiments allows a wide variety of conditions to be investigated. The results presented in section 3.3 were obtained by slowly varying the applied torque amplitude at a set torque order. Results for both a single absorber system and a multi-absorber system are presented. A photograph of the rotor assembly and absorbers is shown in Figure 3.1, and a schematic diagram of the experimental apparatus is shown in Figure 3.2. The main component of the experimental apparatus is a servo motor (D) that drives a shaft with an attached flywheel (H). The shaft is constrained by two bearings, one above and one below the flywheel. The absorbers are shown as two solid circles located at opposing sides of the flywheel. The entire assembly is enclosed in an aluminum frame. The remaining components serve as measuring or control devices. Specifically, the torque is controlled through a feedback system (F) that monitors the motor current. The command signal for this system comes from two sources, the computer (B) and the signal generator (E). The computer maintains the mean speed of the rotor at Ω and the signal generator is used to supply the fluctuating torque components. The signal generator receives its time base from an encoder on the motor that produces 1000 pulses per revolution. By selecting the number of pulses per period, it is possible to excite the system at any prescribed order. This feature of the system allows torque fluctuations to be applied that are any prescribed function of the angular position of the rotor.

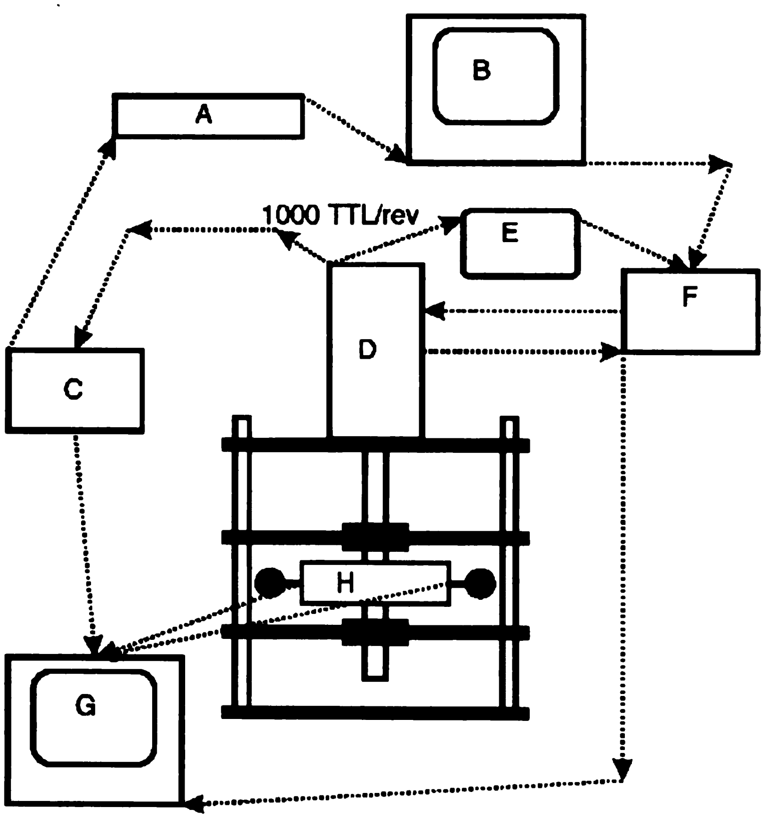

Figure 3.2: Schematic diagram of the experimental apparatus.

The remaining components shown in Figure 3.2 are a frequency to voltage converter (C), a computer (G), and a low pass filter (A). The frequency to voltage converter is used to measure the instantaneous speed of the rotor. This signal is sent to both computers (B and G). However, before being sent to the computer that controls the mean speed of the rotor (B), the signal is sent through a low pass filter. The computer (B) then uses a PI-controller to control the low frequency drift in the rotor's mean speed. This method of controlling the rotor's mean speed was chosen to isolate the effect of the higher frequency speed variations that are caused by the applied fluctuating torque. The second computer (G) is used to monitor and record the experimental data in conjunction with a signal analyzer.

The absorbers' response angle is measured using quadrature encoders. Each absorber has an encoder attached to it. The encoder signals are connected to the computer (G) through a slip ring and a bank of low pass filters to eliminate the high frequency noise caused by the motor. These signals are converted to an angle measurement by a quadrature decoder board. The computer records the torque level, the rotor speed, and each absorbers' angle at a specified sampling rate. The physical system used is shown in Figure 3.1. The rotor, absorbers, servo motor, and the enclosure are all visible in this figure. A schematic of the rotor and two absorbers is shown in Figure 2.1. Although only two absorbers are pictured, the rotor's design allows for up to four absorbers to be simultaneously attached.

3.2 Parameter Identification

Before the experimental results can be compared with the predictions from the averaged equations predictions and the numerical results obtained by simulating the fully nonlinear equations, various physical parameters must be obtained so that the experimental results can be properly scaled. These parameters were obtained using both direct measurements such as lengths and masses and more involved tests to quantify the absorber damping, absorber orders, and the rotor inertia. The length and mass measurements were measured directly and are tabulated in Table 3.1.

The absorbers' tuning orders were measured experimentally by measuring the period of the absorbers with the rotor spinning at a known mean speed. The absorbers' radii of gyration about their centers of mass were calculated using the measured absorber orders, the measured values for r and R, and Equation 2.7. The ρ values are included in Table 3.1.

There is some unavoidable experimental uncertainty in the parameters in Table 3.1. The values listed were chosen from within the range of measured values so that the experimental results matched the simulation results as well as possible. The measured values in Table 3.1 were used to calculate the parameters listed in Table 3.2. The simulation results and the theoretical curves were very sensitive to small changes in ε, r, and R. Simply changing the number of significant digits retained for these parameters had a very pronounced effect on the results obtained.

The rotor's inertia with all four absorbers attached and locked was calculated using the relationship:

$$T = J\ddot{\theta} \tag{3.1}$$

By using equation 3.1 and measuring the torque and the rotor's angular acceleration, the inertia of the rotor and the four locked absorbers was found to be 0.104248 kg.m^2. Using these measurements and the expression for ε given in Chapter Two, ε is found to be 0.0517 for the case when one absorber is active and four times that value, 0.208 for the case when four absorbers are active. This is the "small" parameter that is used in the scaling analysis performed in Chapter Two.

The damping ratios were obtained by assuming that the primary damping mechanism is viscous damping. The precise values of the damping ratio for each absorber were obtained by utilizing the log decrement method. The procedure used to quantify the damping ratios for each absorber is outlined in Appendix 1. The damping ratios for each absorber are also listed in Table 3.1.

Item	Description	Range	Value Used
R	Distance between flywheel center and point around which the absorber rotates	0.120±0.002m	0.118m
r	Distance from point around which absorber rotates to absorber C.M.	0.04±0.001m	0.039m
$\tilde{n}$	CPVA Order for Absorber 1	1.316±0.005	1.316
	CPVA Order for Absorber 2	1.320±0.005	1.320
	CPVA Order for Absorber 3	1.320±0.005	1.320
	CPVA Order for Absorber 4	1.330±0.005	1.330
J	Flywheel inertia with all four absorbers locked	0.1034-0.1061 kg/m^2	0.1042 kg/m^2
m	Absorber mass	0.260±0.005N	0.255 N
N	Number of Absorbers		1,4
Ω	Rotor mean Speed		10 π rad/s
ζ_1	Damping ratio for absorber 1	.00241-.005044	0.02041
ζ_2	Damping ratio for absorber 2	.01512-.02119	0.0212
ζ_3	Damping ratio for absorber 3	.003658-.004086	0.00365
ζ_4	Damping ratio for absorber 4	.03227-.04371	0.0322

Table 3.1: Measured physical parameter values of CPVA system.

Item	Description	Value
R_0	Distance between flywheel center and absorber center of mass	0.1570m
ρ_1	Radius of gyration about absorber C.M for absorber 1	0.0337m
ρ_2	Radius of gyration about absorber C.M for absorber 2	0.0335m
ρ_3	Radius of gyration about absorber C.M for absorber 3	0.0335m
ρ_4	Radius of gyration about absorber C.M for absorber 4	0.0329m
ε	Inertia ratio	0.052, 0.21

Table 3.2: Calculated system parameters.

Measured Item	Physical Meaning	Measured Quantity	Multiplication Constant	Desired Value
T_θ	Fluctuating torque amplitude	Spectrum amplitude [mV]	$0.01857/(J\Omega^2)$	Γ_θ
$\dot{\theta}$	Instantaneous Flywheel velocity	Spectrum amplitude [mV]	$2n\pi\Omega/1000$	$\ddot{\theta}$
$\dot{\theta}$	Instantaneous Flywheel velocity	Spectrum amplitude [mV]	$2n\pi / (1000\Omega^2)$	vv'

Table 3.3: Calibration constants used to convert experimental measurements into physical quantities.

Table 3.3 shows some important calibration constants that are needed in order to relate the measured quantities to the non-dimensional values used in the analytical results. In Table 3.3, spectrum amplitude refers to the amplitude of the power spectrum at the order of interest.

Using Tables 3.1, 3.2, and 3.3, it is now possible to scale the experimental results and compare them with numerical simulations of equation 2.20 and approximate theoretical results from equations 2.30 and 2.34. The next section will show these results for the case when a single absorber is active.

3.3 Experimental Results for One Active Absorber

In this section, a series of representative experimental results will be presented. These results were obtained by slowly varying the applied fluctuating torque amplitude at a specific torque order and measuring the conditions at the resulting steady-state. The data was then compared to simulation results and theoretical predictions for the same torque order. Figures 3.3, 3.5 and 3.6 all show comparisons of the approximate theoretical, experimental, and simulation results of absorber arc-length response for different torque orders. Figures 3.4, 3.7, and 3.8 show the corresponding angular acceleration curves. The experimental results clearly possess the hysteretic behavior described in Chapter Two.

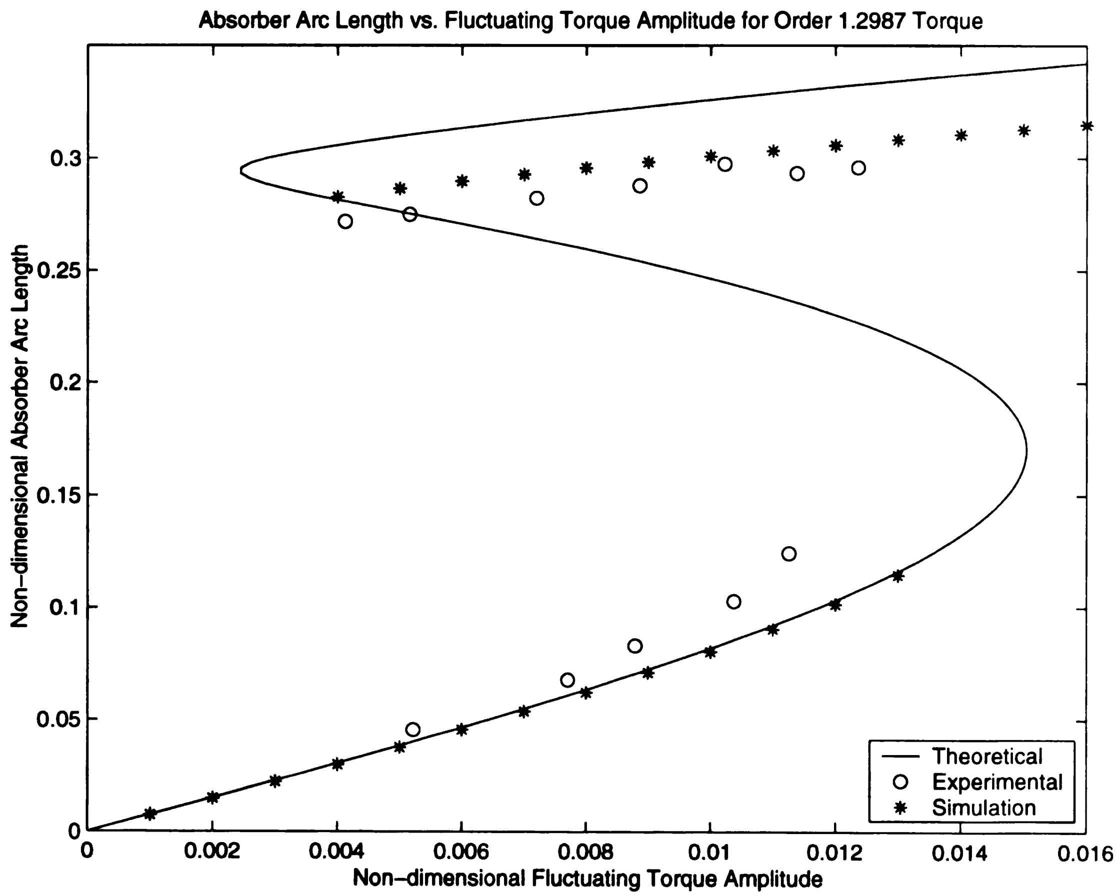

Figure 3.3: Absorber arc-length amplitude versus non-dimensional torque, Γ_θ, for forcing order 1.2987.

The case considered in Figure 3.3 is very close to perfect tuning, σ=0.26, which is why the experimental, theoretical, and simulation results all jump at such a relatively low torque amplitude compared to Figures 3.5 and 3.8. The experimental results in Figure 3.3 clearly possess the same qualitative shape as the theoretical and simulation results. As Figure 3.3 shows, the experimental and simulation torque amplitudes at which the jump bifurcations occur match reasonably well. The hysteresis effect is clearly shown in Figure 3.3. The tailing up of the absorber response amplitude near the jump point could be related to the nonlinear damping that is present in the system. Figure 3.4 shows the angular acceleration results that correspond with the absorber results shown in Figure 3.3.

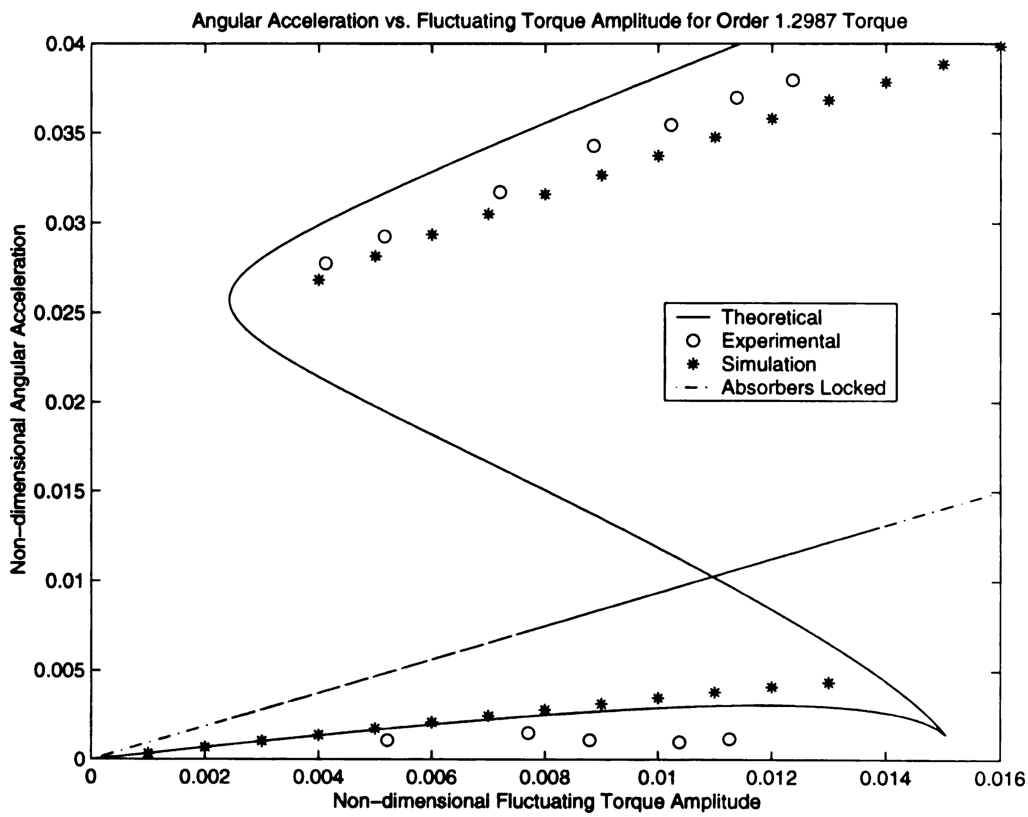

Figure 3.4: Angular acceleration of rotor, vv', versus non-dimensional torque, Γ_θ, for forcing order 1.2987.

The experimental angular acceleration data clearly shows that the absorbers have improved the torsional vibrations in the rotor over a specific range of applied torques. Because of the form of equation 2.30, we expect that larger absorber responses on the lower branch will result in lower rotor angular accelerations. This is consistent with Figure 3.3 where the experimental rotor response was larger than the theoretical or simulation results, and the experimental angular acceleration measurements are lower than the corresponding theoretical and simulation values.

Figure 3.8 shows the absorber response for applied torques of order 1.282. This case is still close to perfect tuning, σ=0.51. The increase in the detuning resulted in a much larger range over which the absorbers were absorbing torque. Figures 3.5, 3.6, and 3.7 shows the absorber arc length versus rotor angle, the non-dimensional torque signal versus rotor angle, and the non-dimensional rotor speed versus rotor angle, respectively.

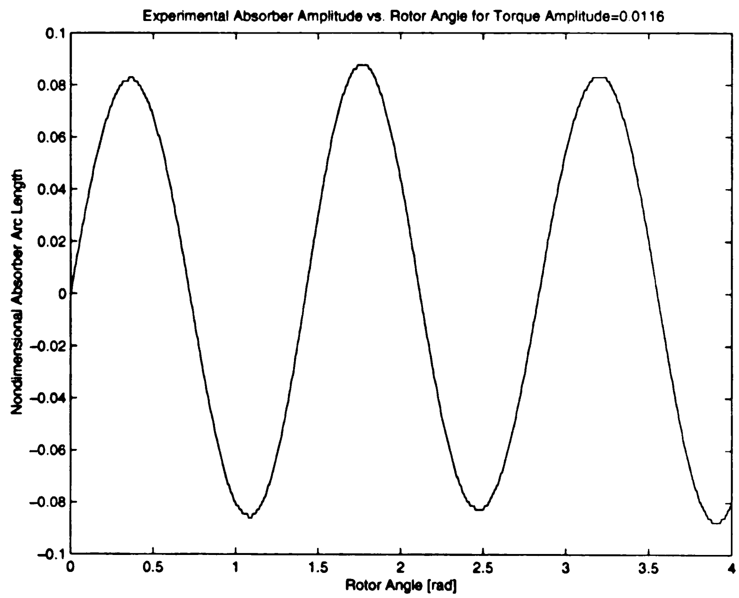

Figure 3.5: Absorber arc length versus rotor angle for fluctuating torque amplitude of 0.0116 and torque order 1.28205.

Figure 3.6 shows the torque amplitude plotted versus the rotor angle. This torque signal is the sum of the T_0 and T_θ.

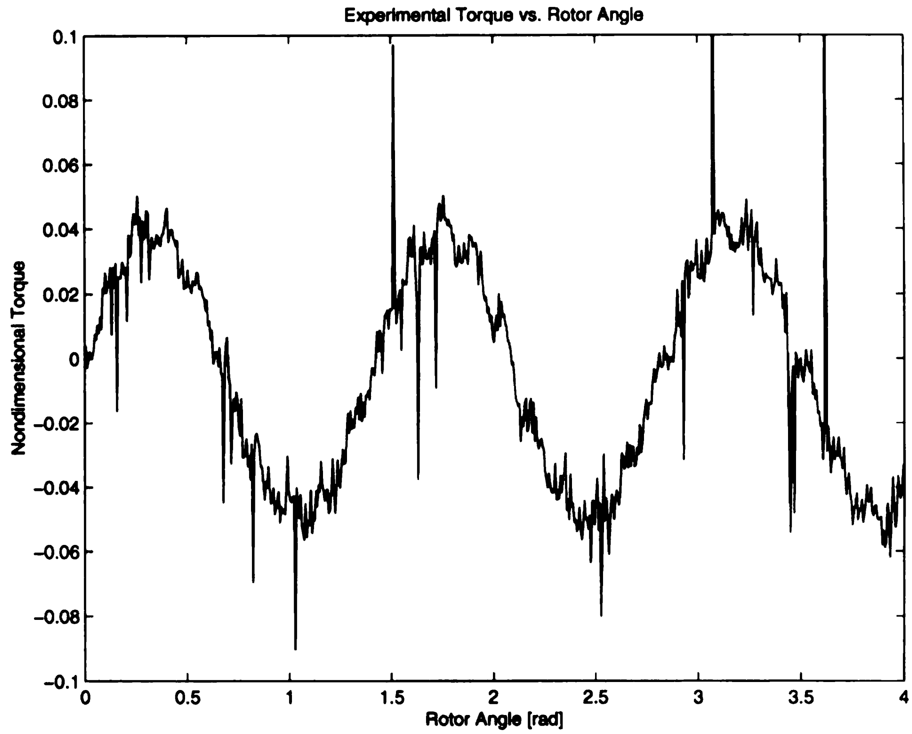

Figure 3.6: Non-dimensional experimental torque versus rotor angle for fluctuating torque amplitude of 0.0116 and torque order 1.28205.

Figure 3.7 shows the non-dimensional rotor speed versus rotor angle for the same operating conditions as Figures 3.5 and 3.6. The data presented in Figures 3.7 and 3.6 was not filtered, so the high frequency noise is still present in the signals plotted. This noise did not affect the comparison of the experimental absorber amplitudes or angular acceleration to the theoretical and simulation values because the angular acceleration and torque values were obtained by measuring the spectrum amplitude of the instantaneous speed signal and the motor current using a FFT analyzer. The amplitudes of interest in the instantaneous speed signal and the motor current signal were then converted to an angular acceleration amplitude and a torque amplitude, respectively. By using the FFT analyzer to isolate the harmonics of interest, the high-frequency noise present in the instantaneous speed signal and the torque signal was essentially filtered out of the signals.

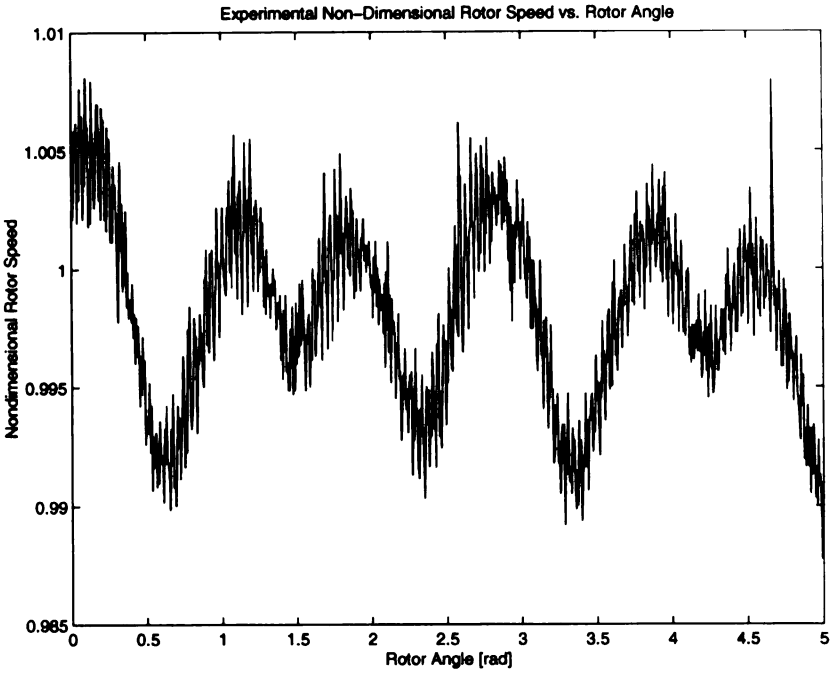

Figure 3.7: Non-dimensional rotor speed versus rotor angle for fluctuating torque amplitude of 0.0116 and torque order 1.28205.

Figure 3.8, like Figure 3.3, shows that the experimental absorber response measurements are comparable to the theoretical and simulation results. The discrepancy between the experimental results and the simulation results is attributed to the extremely sensitive nature of the system with regards to the scaling parameters. Figure 3.9 shows an alternative way of looking at the absorber response data. In this curve, the absorber's non-dimensional arc length has been normalized by the associated non-dimensional fluctuating torque amplitude. The result is a type of "gain" parameter. Figure 3.9 shows that the experimental results match the simulation results well on both the lower branch and the upper branch of the solution curve. Figure 3.9, like Figure 3.8, shows that the experimental results begin to deviate from the analytical results near the jump point. Figure 3.10 shows the angular acceleration data that corresponds to the absorber responses shown in Figures 3.8 and 3.9.

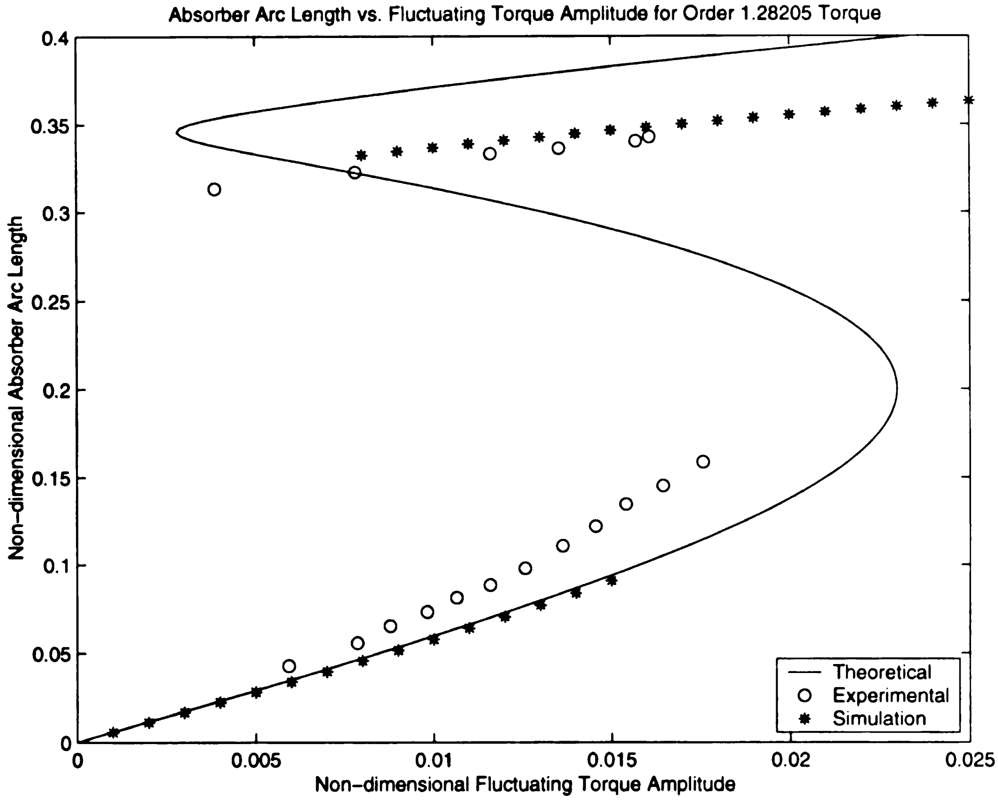

Figure 3.8: Absorber arc-length versus fluctuating torque amplitude for order 1.28205 torques.

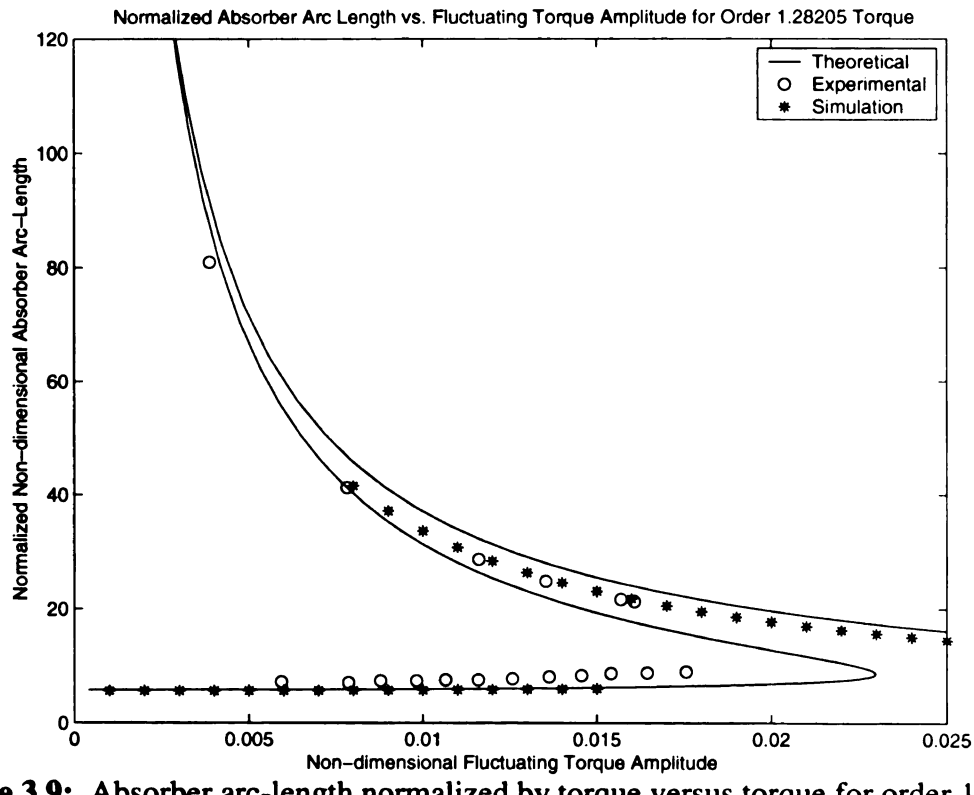

Figure 3.9: Absorber arc-length normalized by torque versus torque for order 1.28205 torques.

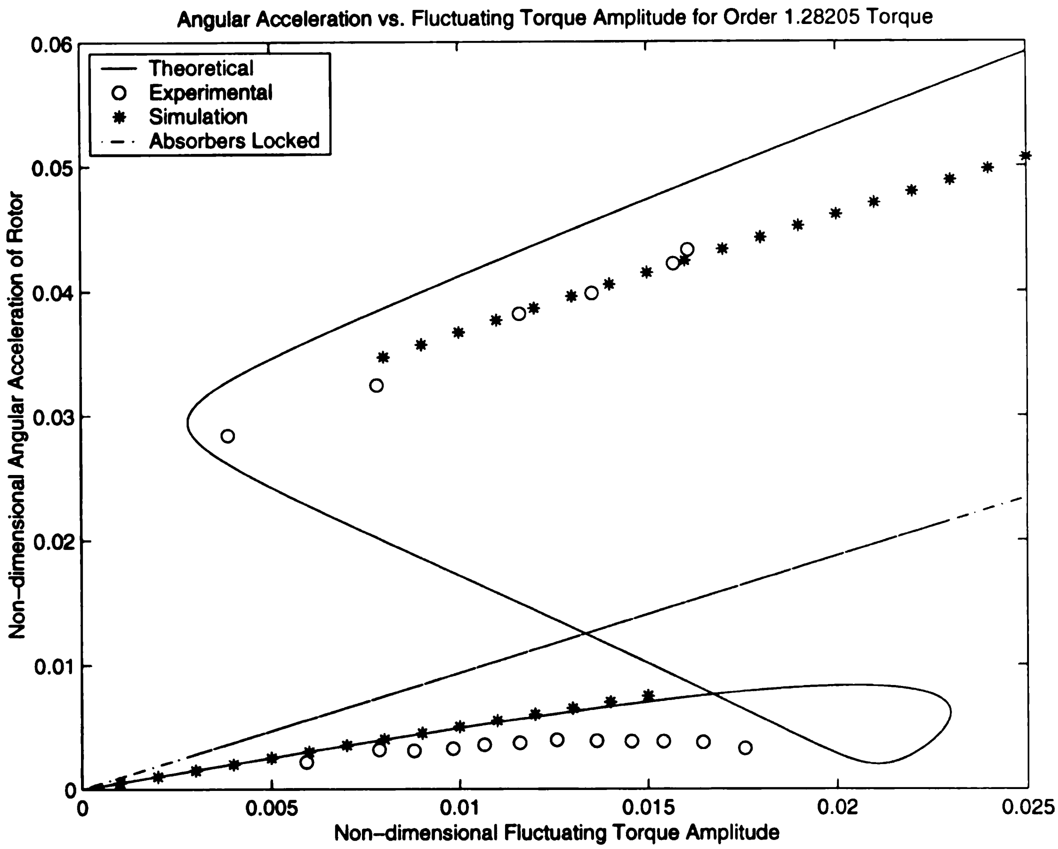

Figure 3.10: Angular acceleration versus fluctuating torque amplitude for order 1.28205 torque.

Figure 3.10 shows that the experimental angular acceleration is below the analytical values on the lower branch of the solution curve. But, as was the case in Figures 3.3 and 3.4, the fact that the experimental absorber response was larger than the analytical value suggests that the experimental angular acceleration will be lower than the analytical predictions. Figure 3.10 also clearly shows that the CPVA's noticeably reduce the torsional vibrations over an operating range comparable to that predicted by simulation results.

Figures 3.11, 3.12, and 3.13 show results for torque order 1.255, corresponding to σ=0.945. These plots show how the experimental system with the pendulum overturned by 5%, an amount commonly used in industry to extend the operating range, compares to the analytical results.

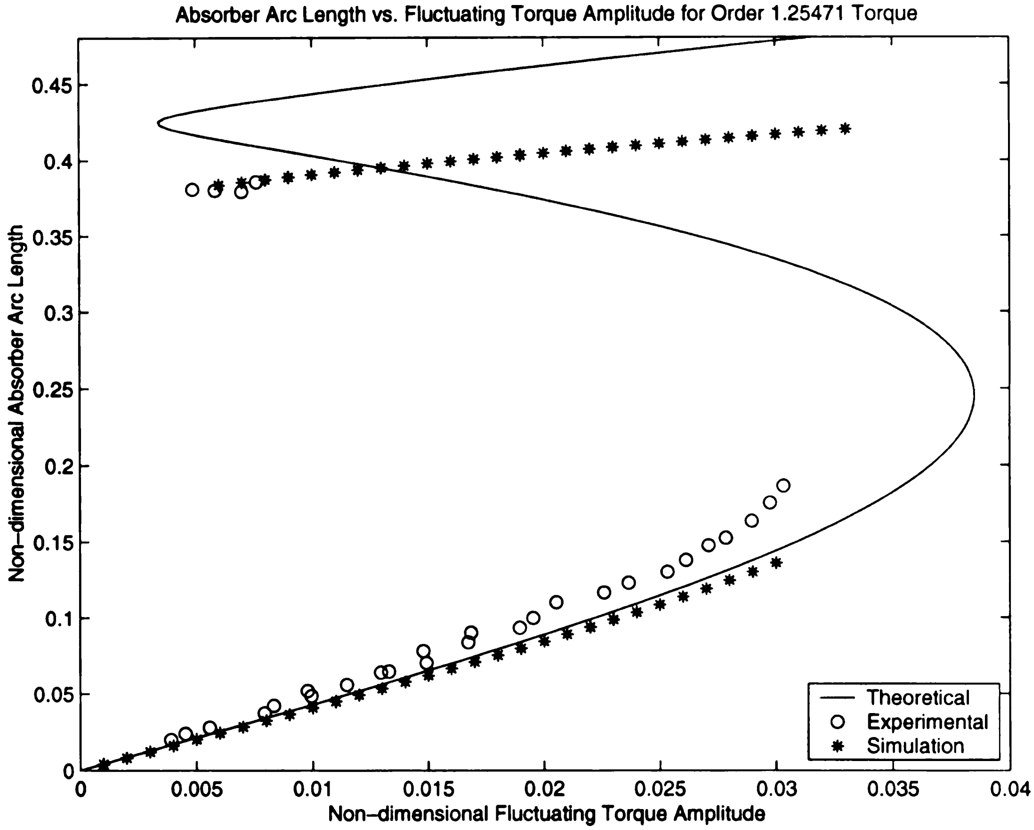

Figure 3.11: Absorber arc-length versus non-dimensional fluctuating torque amplitude for order 1.25471 torque (5% overtuning).

Figure 3.11 shows that the experimental absorber response agrees well with the simulation and theoretical results. Figures 3.3, 3.5, and 3.11 show a surprising trend. As the amount of mistuning increases, the experimental results match the simulation and theoretical results better. Because the theoretical predictions are based on approximations that assume that the torque orders are close to the absorber order, it was expected that the experimental absorber results would match the analytical results better for lower detuning values than for larger detuning values.

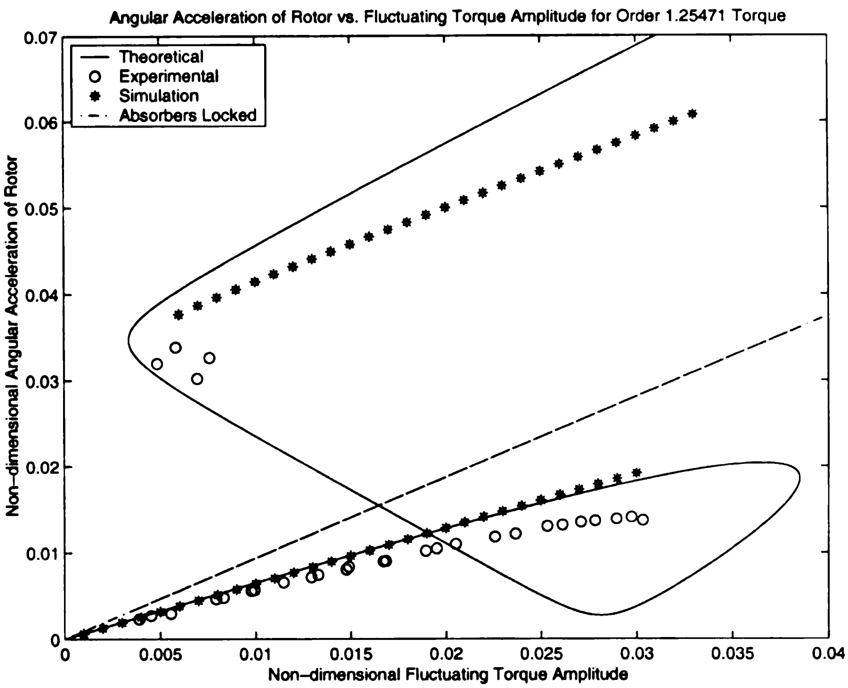

Figure 3.12: Angular acceleration versus non-dimensional fluctuating torque amplitude for order 1.25471 torques.

Figure 3.12 shows the angular acceleration results that correspond to the absorber response results shown in Figure 3.11. Figure 3.12 illustrates that the experimental angular acceleration results agree well with the analytical predictions. This was expected because of how well the experimental and analytical absorber responses agreed. In Figures 3.11 and 3.12, the torque amplitude that caused the absorbers jump in both the experiments and the simulations is seen to match very well, but differs from the theory. The difference between the torque amplitude at which the theoretical curve predicts the jump point will occur and the torque amplitude at which the jump point occurs in the simulations and experiments results from the fact that the theoretical curve is an approximation of the nonlinear equations. As the pendulum response gets large, the approximate theoretical solution begins to diverge from the solution to the fully nonlinear equations. The next plot shows the same data presented in Figure 3.12, but the angular acceleration values have been normalized by the non-dimensional torque amplitudes.

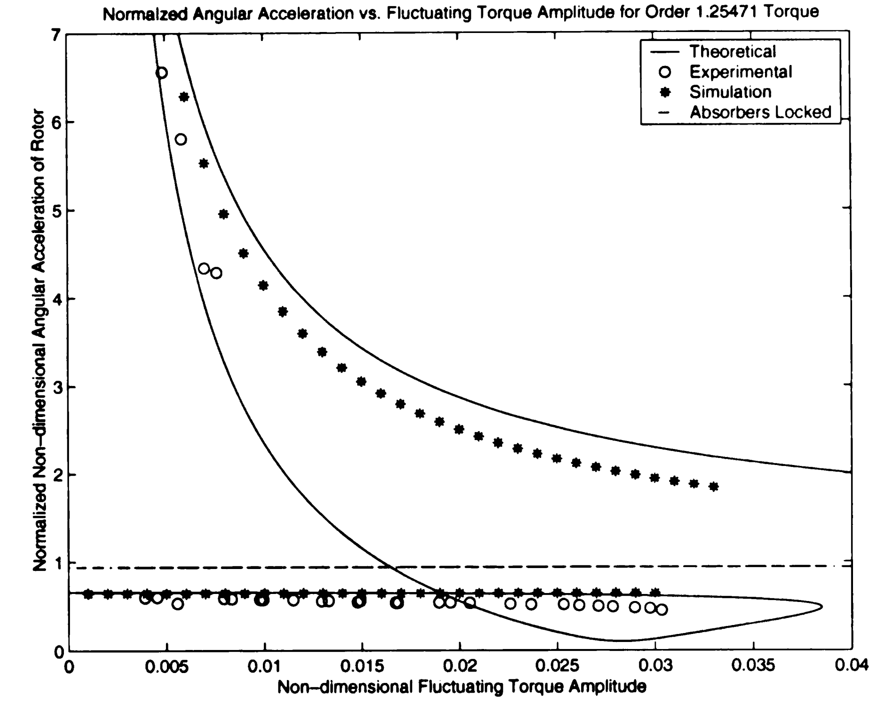

Figure 3.13: Normalized angular acceleration versus fluctuating torque amplitude for order 1.25471 torques.

Figures 3.13 and 3.12 both show that the system with an active CPVA has lower angular accelerations for a quite wide operating range when compared to the system with the absorbers locked.

3.4 Experimental Results for Four Active Absorbers

Space considerations and rotational imbalance issues often limit the size of CPVA's that can be attached to a rotor. Because the largest single absorber that can be used is often not large enough to lower torsional vibrations to satisfactory levels and because single absorbers often cause balance problems, systems of multiple absorbers are often attached to rotors. These absorbers are tuned to the same order, to within manufacturing tolerances. Experimental results are shown below which indicate the complex dynamics that can occur in these types of installations.

All of the complex dynamics occurred near the perfect tuning location. Far from tuning, the absorbers responded in a unison fashion, behaving essentially like a single absorber. Figures 3.14, 3.15, 3.16, 3.17, and 3.18 show results for four active absorbers when the system is excited by order 1.2987 torques, which corresponds to an average detuning value of σ=0.339, with a range of σ=0.232-0.438.

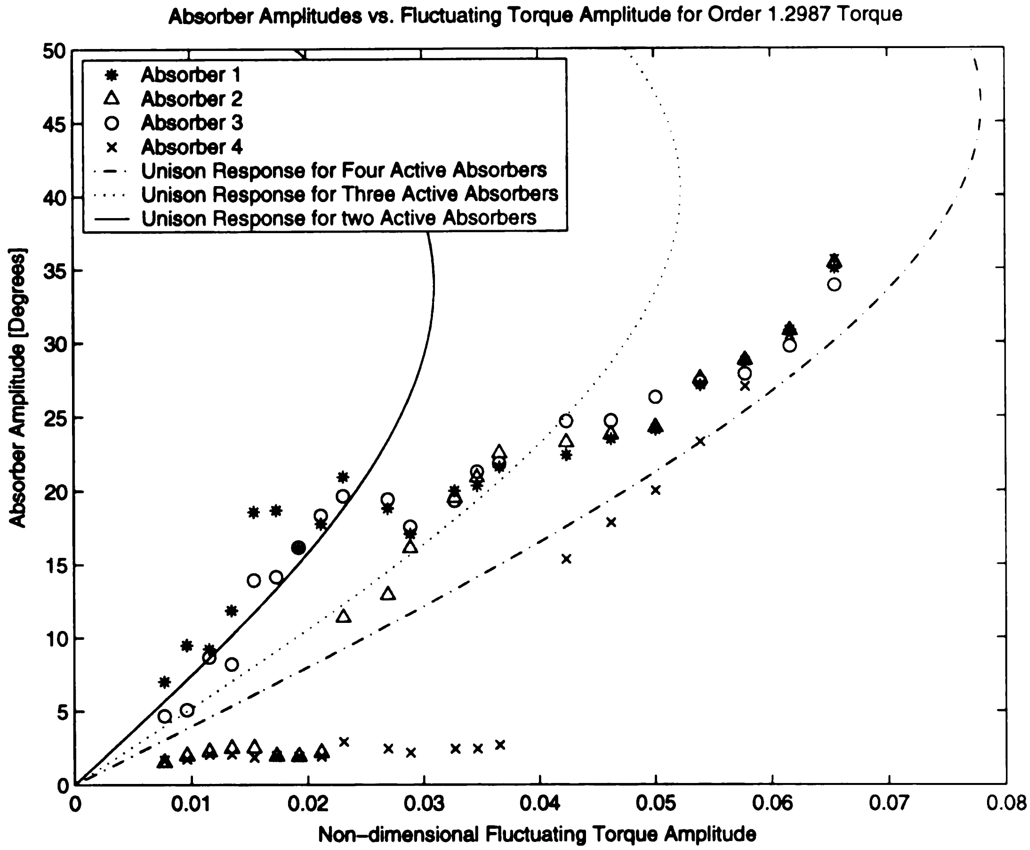

Figure 3.14: Absorber amplitudes versus fluctuating torque amplitude for order 1.2987 torques.

The general features of the absorber responses to increasing torques shown in Figure 3.14 was seen in numerous experiments. A key feature is that as the torque level increases, more absorbers become active. At low torque amplitudes, only absorber one and absorber three were active. As the torque level was increased, first absorber two, and then absorber four, became active at a particular torque level. Figure 3.14 shows that as additional absorbers become active, the slope of the absorbers' increase responses decreases. The absorber responses clearly agree well with the unison response predictions for two absorbers, three absorbers, and four absorbers, when two, three, or four absorbers are active, respectively.

Figure 3.14 only shows absorber amplitude data. In order to see a more complete picture of how the system is operating, an alternative set of coordinates is plotted [26]. These coordinates are the mean of the absorbers' response amplitudes, the amplitude of $\phi_2 - \phi_1$, the amplitude of $\phi_3 - \phi_1$, and the amplitude of $\phi_4 - \phi_1$, where ϕ_i is the angle of the i^{th} absorber. These coordinates illustrate whether or not the absorbers are operating in unison. For example, if all four absorbers are moving in phase with the same amplitude, the mean will show the amplitude of the response, and the other three coordinates will be zero. Figure 3.15 shows the data from Figure 3.14 plotted using these coordinates.

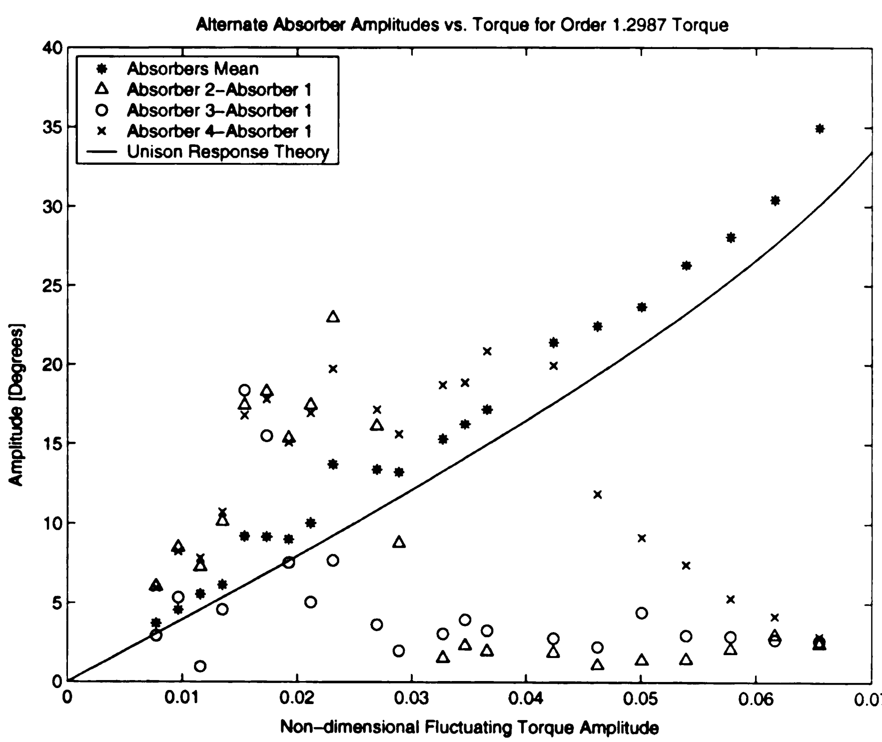

Figure 3.15: Absorber response angles in alternate coordinates versus non-dimensional fluctuating torque amplitude for order 1.2987 torques.

In Figure 3.15, the theoretical unison response curve is plotted using Equation 2.34. Figure 3.15 shows clearly how additional absorbers become active and move into a unison response with the other active absorbers as the torque level increases. It is also apparent that the mean absorber response agrees well with the theoretical unison response curve throughout the operating range, even though the absorbers are not responding in unison throughout the entire range. Figure 3.16 shows the angular acceleration data that corresponds to the absorber response data shown in Figures 3.14 and 3.15.

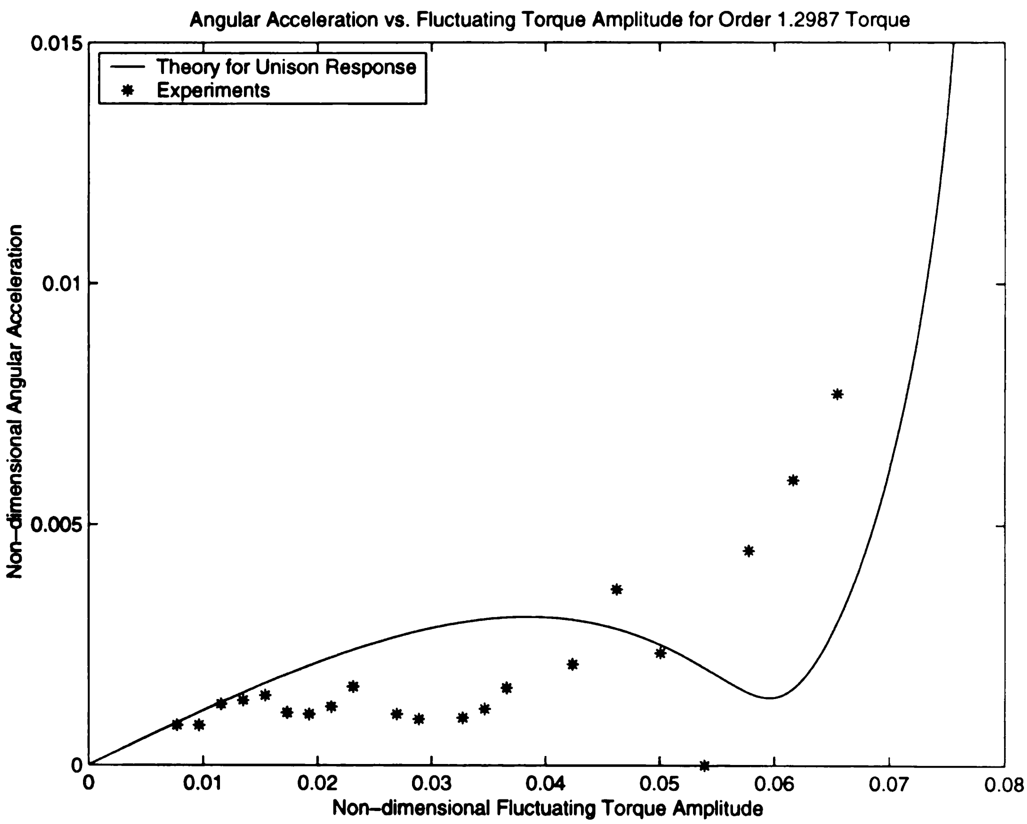

Figure 3.16: Experimental and theoretical rotor angular acceleration versus torque amplitude for order 1.2987 torques.

Figure 3.16 shows that the experimental angular acceleration follows the theoretical prediction reasonably well. The scallops in the experimental angular acceleration at low torque levels correspond with additional absorbers becoming active as the angular acceleration approaches the theoretical curve. This behavior is currently not well understood and deserves and analytical treatment. The next three figures show time traces of the absorbers' responses at specific fluctuating torque amplitudes taken from Figures 3.14 and 3.15.

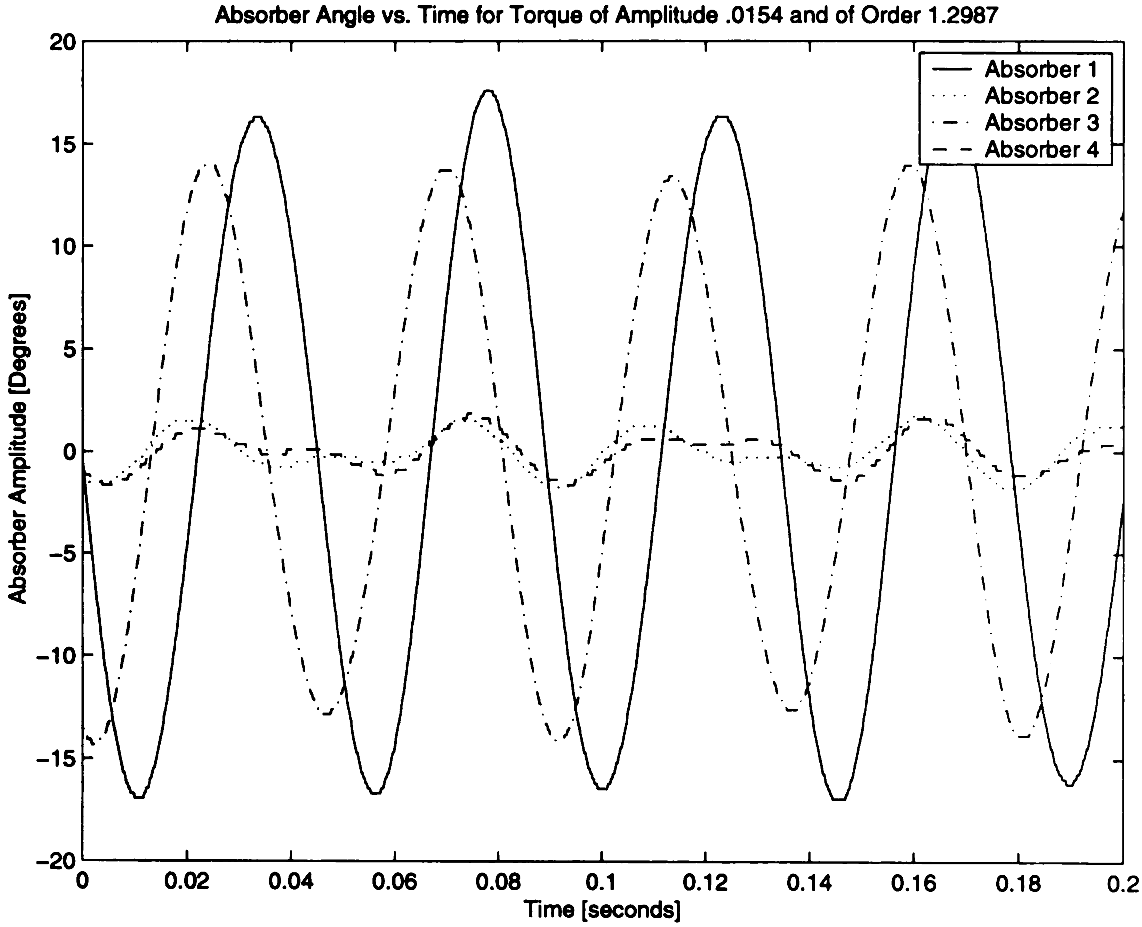

Figure 3.17: Time trace of absorbers' response angle for fluctuating torque amplitude of 0.0154 and torque order 1.2987.

In Figure 3.17, two absorbers are inactive, and two absorbers are active, but not in phase. As the torque amplitude is increased, the two active absorbers begin to move in unison, as shown in Figure 3.18, and at larger amplitudes.

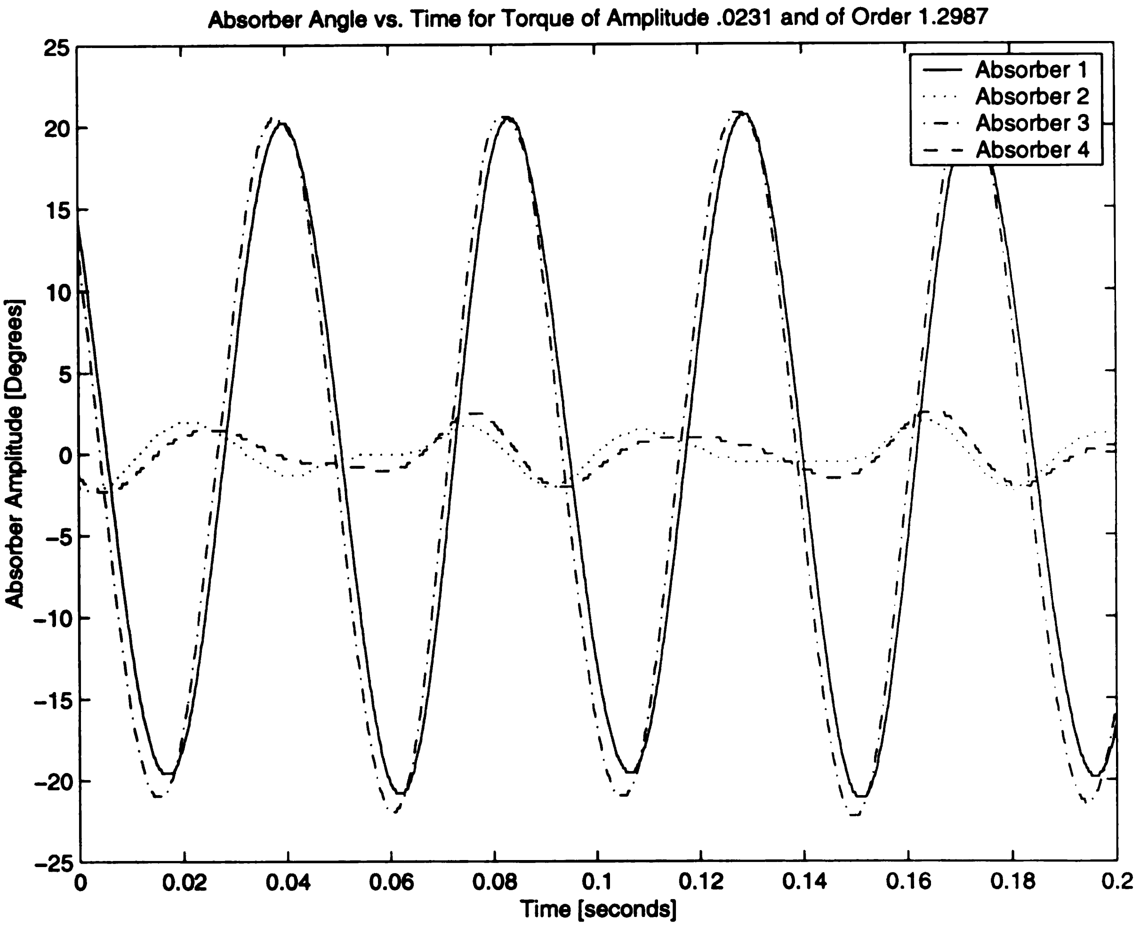

Figure 3.18: Time trace of absorbers' response angle for fluctuating torque amplitude of 0.0231 and torque order 1.2987.

At the torque level shown in Figure 3.17, the two absorbers are moving almost perfectly in phase. The two absorbers that were inactive in Figure 3.16 are still inactive. As the torque level is increased further, another absorber becomes active and begins to move in unison with the two absorbers that are already active. Figure 3.18 shows the time trace for this case when one absorber is inactive and three absorbers are moving in unison.

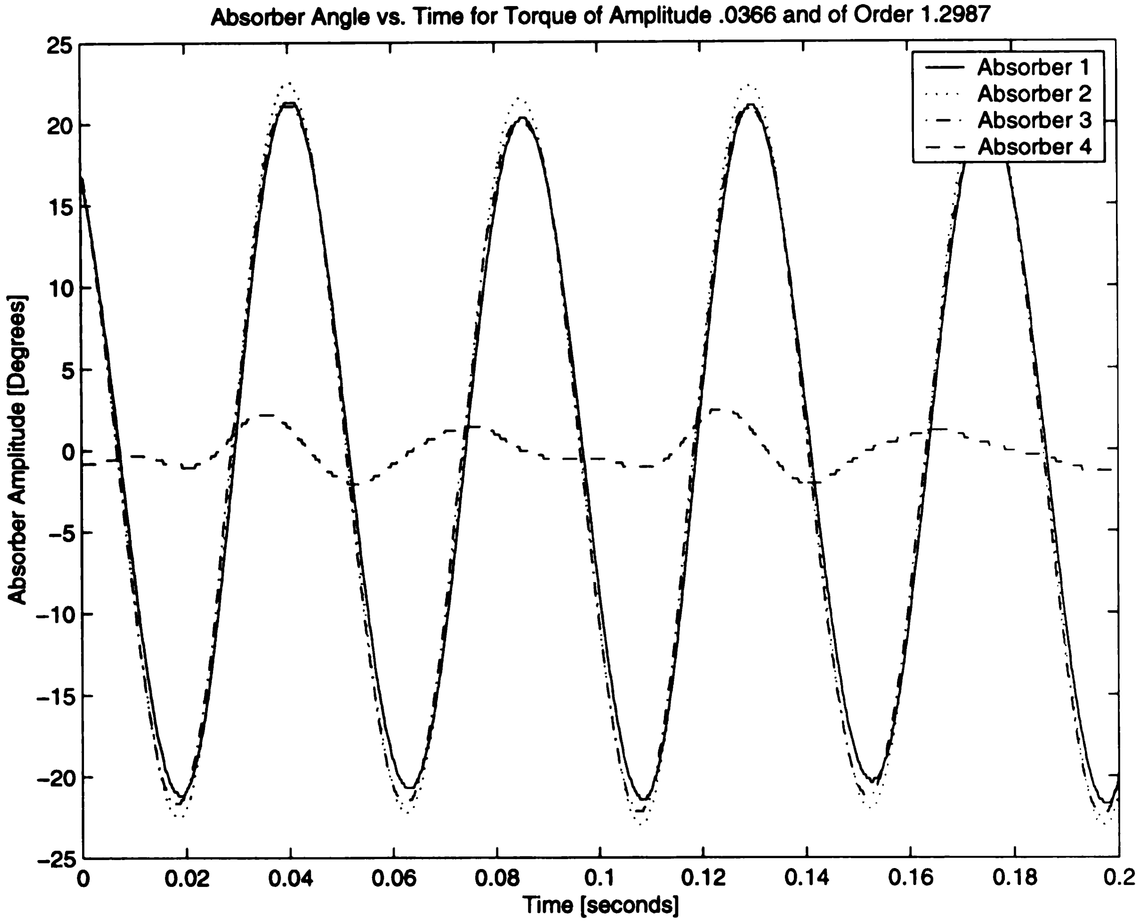

Figure 3.19: Time trace of absorbers' response angle for fluctuating torque amplitude of 0.0366 and torque order 1.2987.

The next series of figures show the results for torque orders closer to perfect tuning than Figures 3.14-3.19. In Figures 3.20-3.22, the order of excitation is 1.3004, which corresponds with an average detuning value of σ=0.313, with a range of σ=0.232-0.438.

Figure 3.20 shows the results for this torque order displayed using the alternate absorber coordinates of Figure 3.15. The same general behavior is visible in Figure 3.20 as was seen in Figure 3.15. Specifically, as the torque amplitude is increased, the absorbers begin to move in a unison fashion. In Figure 3.20, the theoretical unison response curve is visibly turning back and has passed the location of the jump point. The last recorded point in Figure 3.20 clearly shows that the unison response has broken down and the absorbers are no longer moving in a synchronous manner. So, in this case, as predicted by Alsuwaiyan, the absorbers' response became non-synchronous before encountering the jump bifurcation [11]. The non-unison responses closer to zero torque are surprising and were not predicted by Alsuwaiyan.

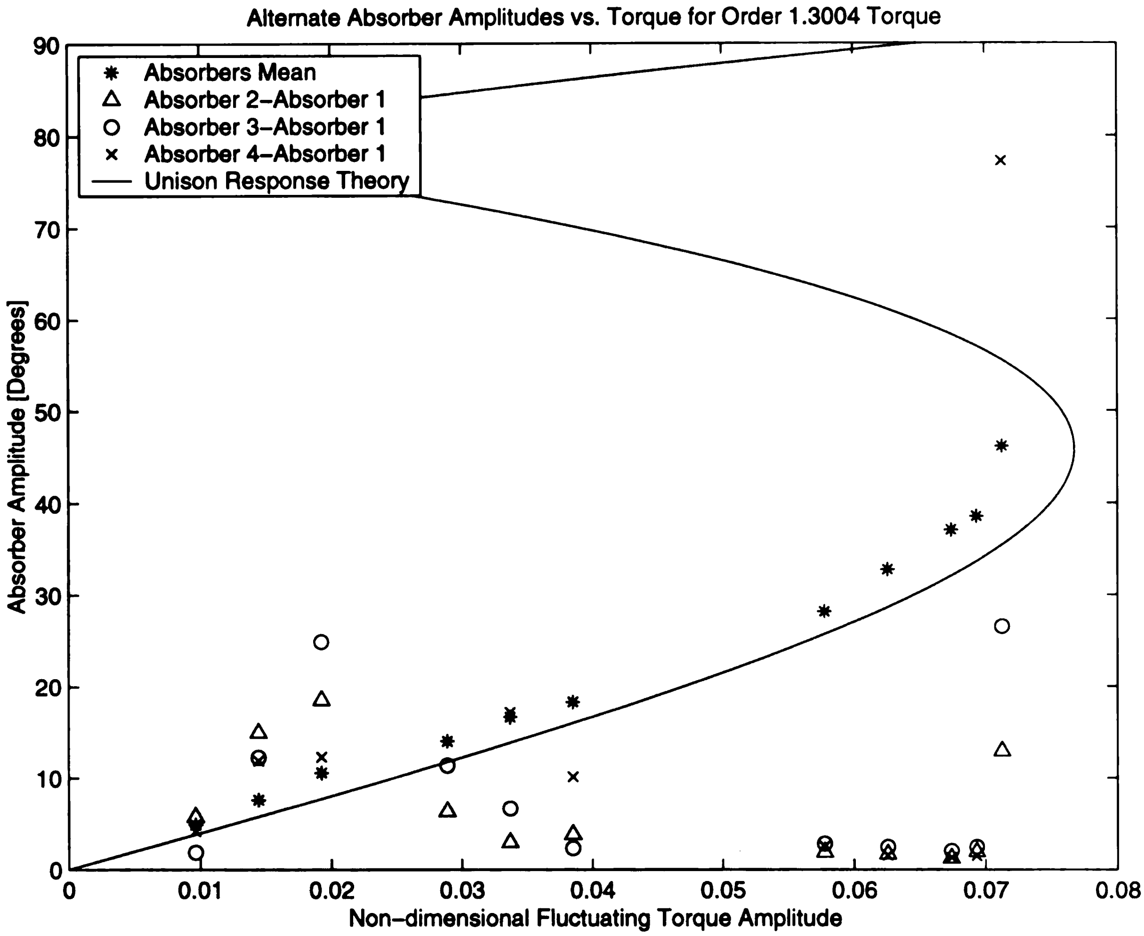

Figure 3.20: Absorber response angles in alternate coordinates versus non-dimensional fluctuating torque amplitude for order 1.3004 torques.

Figure 3.21 shows the same data as Figure 3.20, but plotted in the normal, absorber angle displacement coordinate space. The same key features can be observed in Figure 3.21 as 3.20. Figure 3.21 clearly shows that the unison response breaks down in the last measurement displayed. Figure 3.20 also clearly shows that the absorbers are not synchronous at lower torque levels. Only one data point could be recorded after the unison response broke down because the absorbers began banging into the rotor and the system had to be shut down. This occurrence illustrates the potentially dangerous outcomes that can result if non-unison responses are not accounted for in system designs.

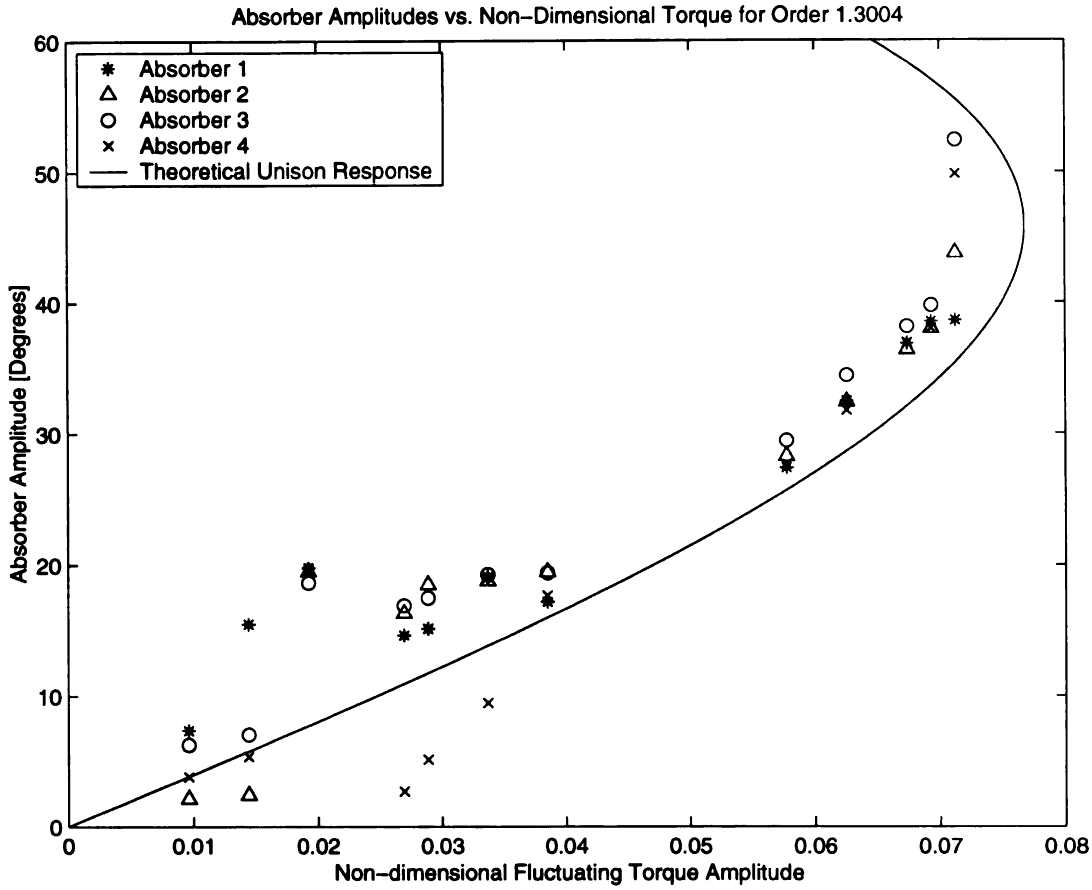

Figure 3.21: Absorber amplitudes versus fluctuating torque amplitude for order 1.3004 torques.

Figure 3.22 shows a time trace that illustrates the advantage of using the coordinates of Figure 3.20. For the case shown in Figure 3.18, the fluctuating torque amplitude is 0.0385, and all four absorbers are active and oscillating with approximately the same amplitude. This information can be read off of Figure 3.21. However, as the time trace in Figure 3.22 shows, one of the absorbers has a phase difference of 180° compared to the other three.

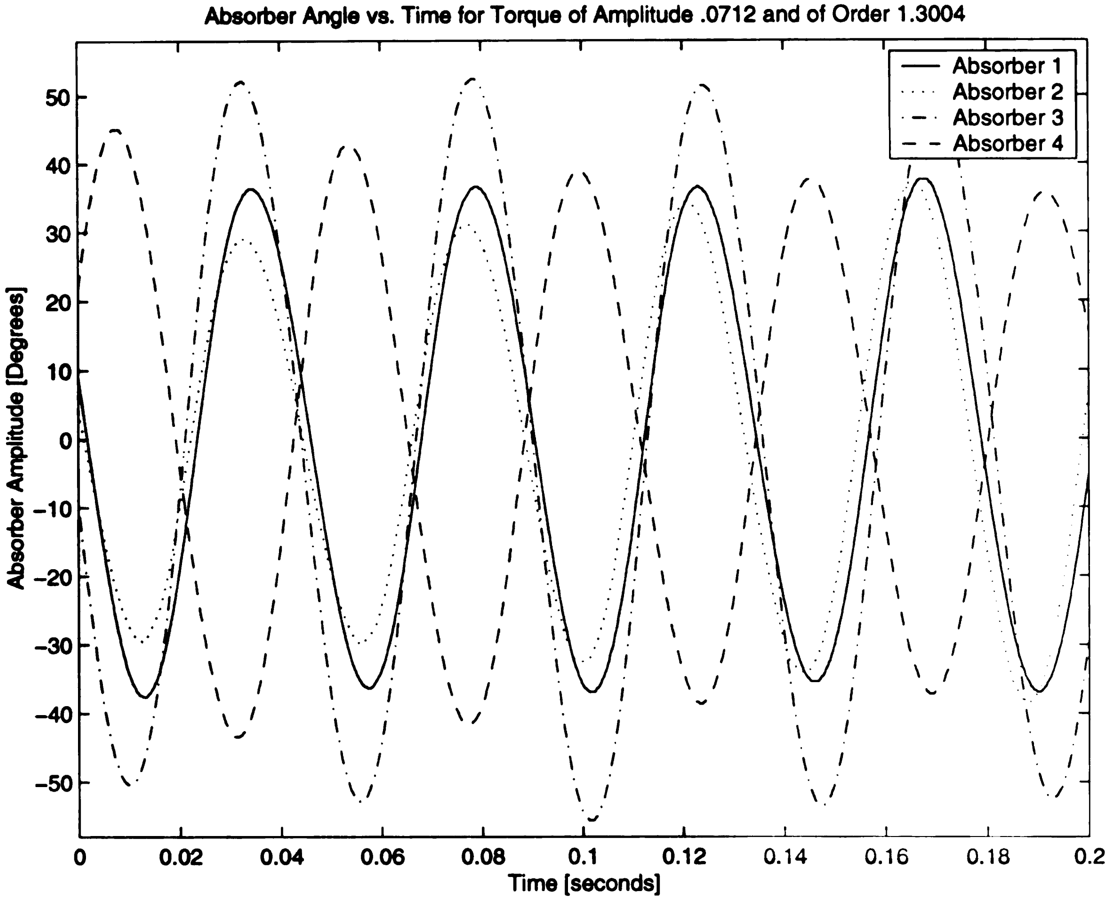

Figure 3.22: Time trace of absorbers' response angle for fluctuating torque amplitude of 0.0361 and torque order 1.3004.

In Figure 3.22, it is worth noting that the absorber that is not in phase with the other three absorbers is the absorber that is furthest from perfect tuning.

Figures 3.23-3.27 show results for order 1.2804 torques, which corresponds to an average detuning value of σ=.619, with a range of σ=0.538-0.745. In Figures 3.23 and 3.24, it is clearly visible that the absorbers migrated first towards the unison response and then away from the unison response as the torque amplitude was increased. The exact pathway for this behavior is not well known, but the absorber with the smallest response amplitude in Figure 3.23 has the largest detuning value. This agrees with our expectations.

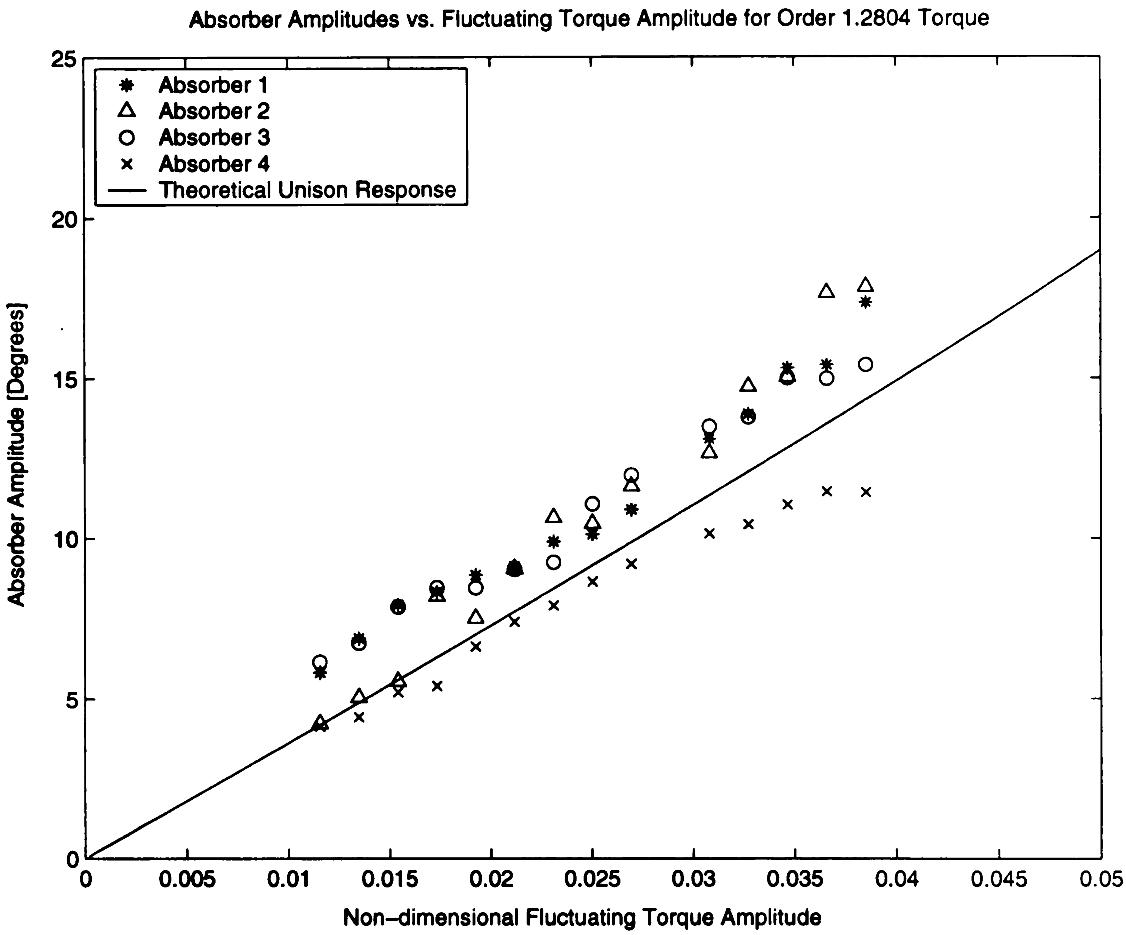

Figure 3.23: Absorber amplitudes versus fluctuating torque amplitude for order 1.2804 torques.

In Figure 3.23, the absorber that was furthest from tuning had a response amplitude significantly below the other three absorbers throughout the test range. Although the response looks mostly unison in Figure 3.23, Figure 3.24 shows that the absorbers converged towards a unison response as the torque was increased, but after the torque amplitude became larger than .03, the unison response began to break down. This divergence is more pronounced when the deviation coordinates of Figure 3.24 are used.

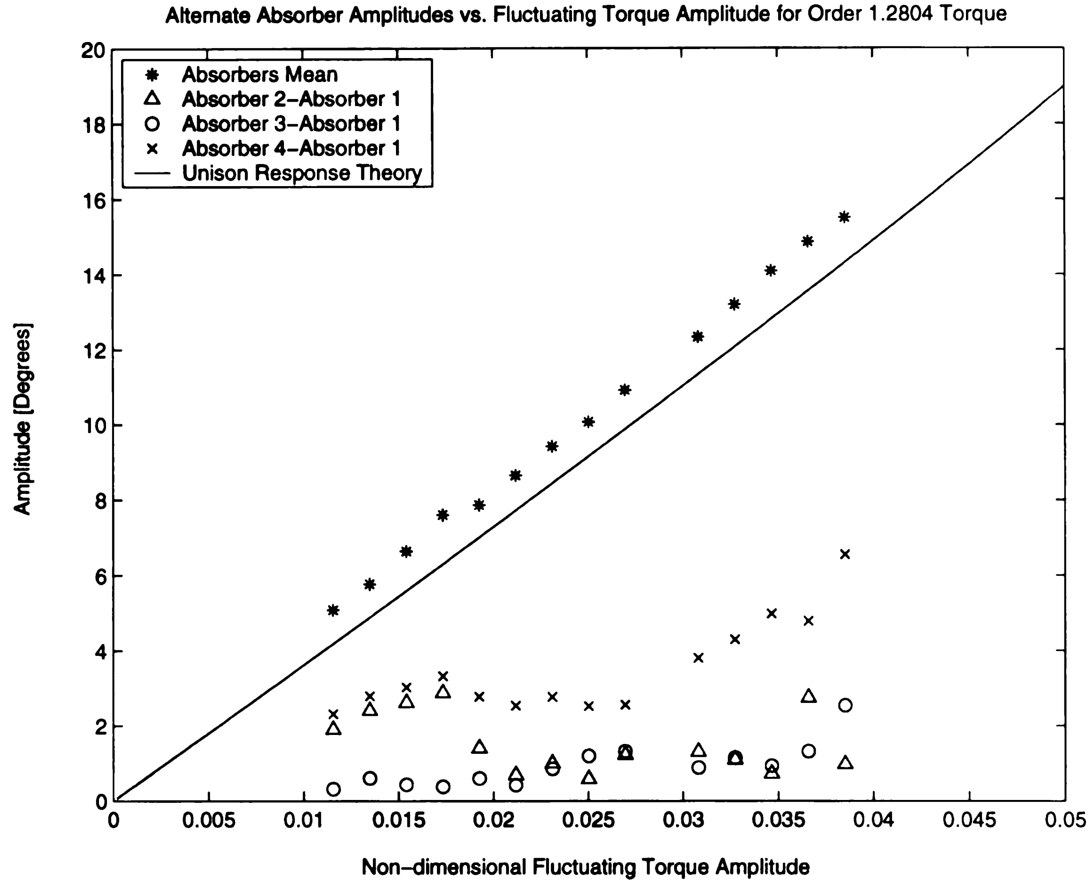

Figure 3.24: Absorber response angles in alternate coordinates versus non-dimensional fluctuating torque amplitude for order 1.2804 torques.

The mean of the absorbers' response amplitudes agrees well with the theoretical prediction throughout the range of torque amplitudes, even when the absorbers are not oscillating in unison. Figure 3.25 shows the angular acceleration data that corresponds with the absorber response data shown in Figures 3.23 and 3.24. At low torque amplitudes, the experimental angular acceleration measurements agree relatively well with the theoretical value for the unison response case. However, the theoretical prediction and the experimental values begin to diverge as the absorbers' response becomes less synchronous.

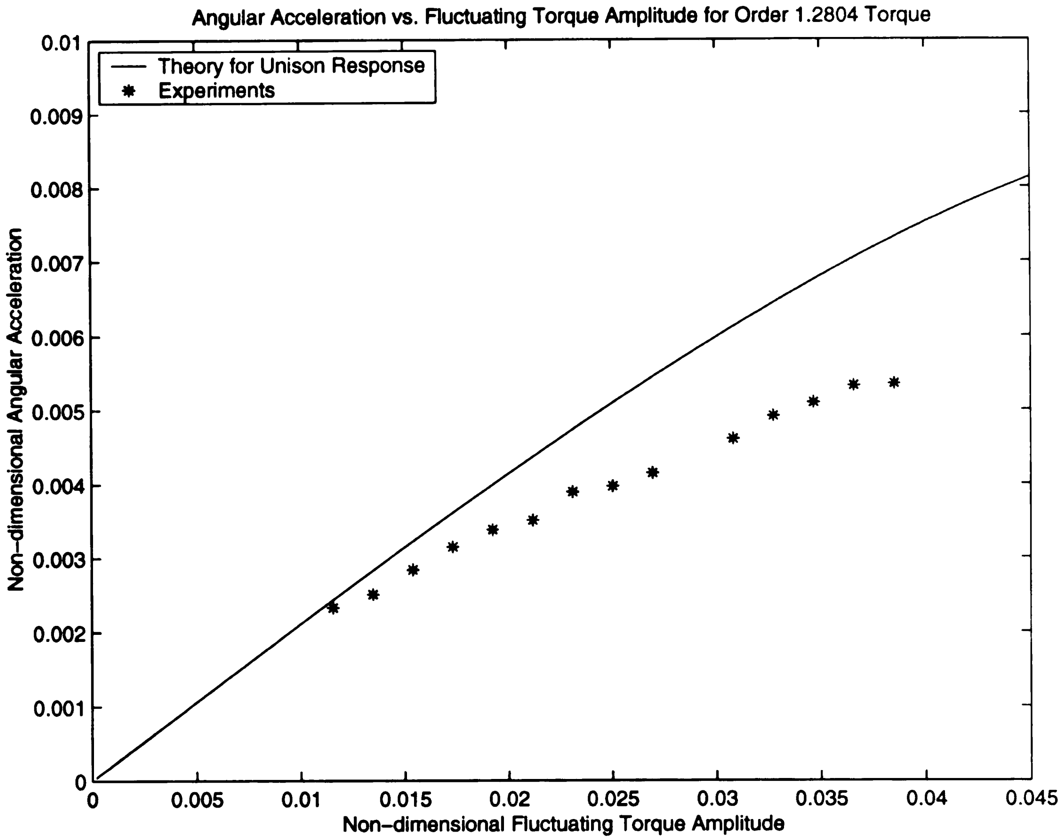

Figure 3.25: Experimental and theoretical rotor angular acceleration versus torque amplitude for order 1.2804 torques.

Figure 3.26 shows a time trace of the absorbers' response for torque amplitude 0.0366 and order 1.2804. The plot shows that even though the absorber amplitudes are not identical, the absorbers are still oscillating in phase. This breakdown in the unison response is not as potentially dangerous as the case shown in Figure 3.22. In Figure 3.26, each of the absorbers is absorbing, but not necessarily the same amount of torque.

Figures 3.23, 3.24, and 3.26 show that not accounting for the possibility of non-unison responses during the design stage can result in potential problems. For order 1.2804 torques, it was shown that the absorber response amplitude was consistently above the amplitude the theoretical unison response amplitude. This could lead to designs in which the pendulum impacts the rotor during operation, which in addition to not functioning as intended, would cause troublesome noise and vibration problems, and reduce the operational torque range.

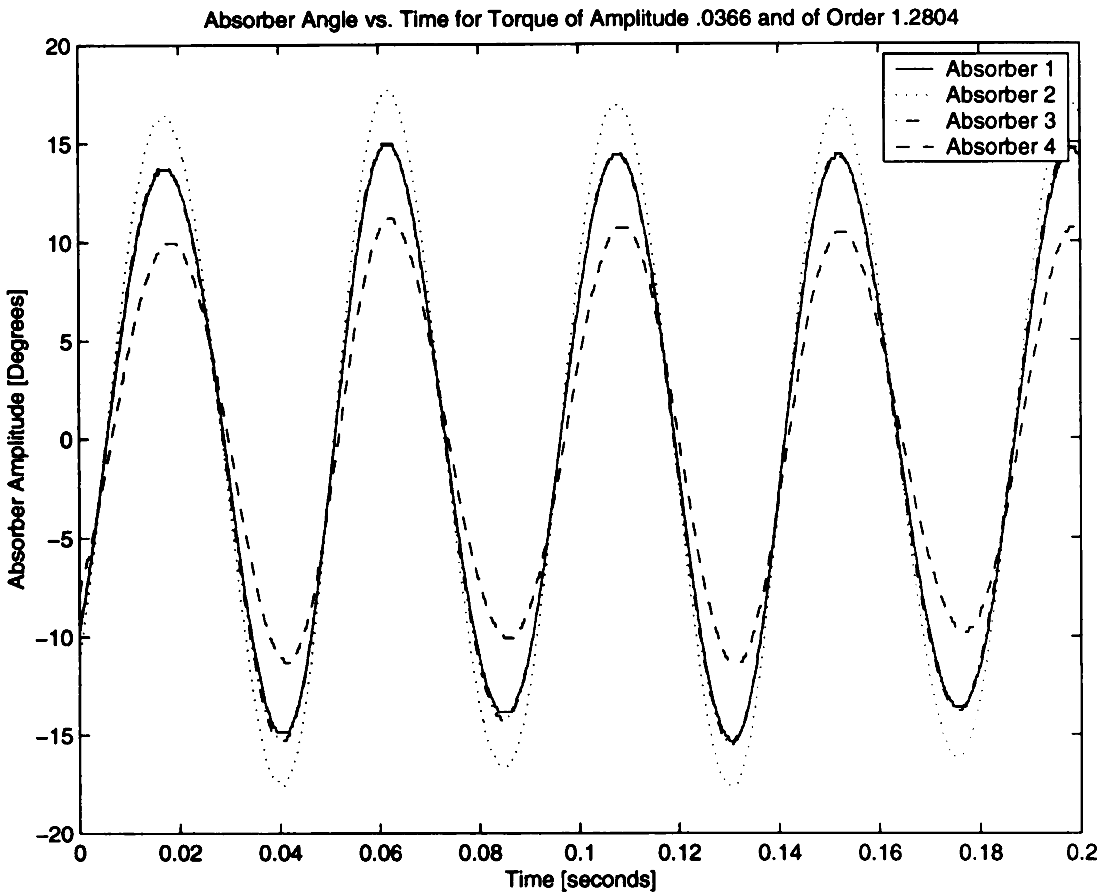

Figure 3.26: Time trace of absorbers' response angle for fluctuating torque amplitude of 0.0385 and torque order 1.2804.

3.5 Summary of Experimental Results

The single absorber experiments were shown to agree well with both the theoretical results and simulation results from previous researchers. The nonlinear jump bifurcation was observed in all of the test cases, and the angular rotation of the rotor was experimentally shown to be reduced over a specific torque range by adding the CPVA's.

The multiple absorber experiments revealed more complicated dynamics than had been expected. Specifically, the system of nearly identical circular-path absorbers used in these experiments was shown to possess numerous non-unison responses. The evolution of the absorbers' responses as the torque amplitude is increased was also not expected. The results presented showed numerous cases where absorbers initially were inactive and then became active and began to move in unison with the other absorbers as the applied fluctuating torque amplitude was increased. Even with these complicated absorber dynamics, the rotor's experimental angular acceleration was shown to agree well with the theoretical prediction based on the unison absorber response case.

CHAPTER FOUR

INTERNAL COMBUSTION ENGINES

In order to improve the fuel economy in large displacement eight-cylinder internal combustion engines, numerous automobile manufacturers are currently investigating experimental engines that operate with different numbers of cylinders active under different operating conditions. These engines are often described as variable displacement engines or displacement on demand engines. The experimental engines used in this study were V8 engines that operated with either eight or four cylinders active.

Four-cycle internal combustion engines produce vibration signals with dominant harmonics at orders equal to the number of active cylinders divided by two, thus during operation in four-cylinder mode, the experimental engines produce vibration signals with a large second order harmonic component. Likewise, in eight-cylinder mode, the dominant excitation harmonic is a fourth order harmonic. However, this is the normal mode of operation for which these engines have been designed to operate. These engines have been well balanced and typically operate smoothly under most operating conditions in eight-cylinder mode. But, during operation in four-cylinder mode (especially idle), the second order vibration levels are above levels acceptable to consumers, so these engines are rendered commercially infeasible due solely to the second order vibrations. Because these vibrations are a function of the engine order and are present throughout the engines' ranges of operating speeds, these types of engines are good applications for CPVA's.

These engines have complicated dynamics and transmit forces to the rest of the automobile through numerous pathways. The experiments reported in section 4.1 verified that the vibration levels are lower in the vehicle with CPVA's attached to the crankshaft than in the vehicle without CPVA's. The purpose of the experiments reported was to assess the effectiveness of CPVA's by comparing the vibration measurements at specified locations in two vehicles, one with CPVA's and one without CPVA's. Both vehicles were operated with the engine idling in both eight and four cylinder modes for various operating conditions.

A V8 engine was manufactured with circular path CPVA's attached to the crankshaft, similarly to previous research efforts [20, 23]. These CPVA's were used in place of the two large round counterweights normally on the crankshaft, and designed such that the total rotational inertia of the two engines was the same. The pendulums were tuned, according to the guidelines of Newland , to order 2.15, that is 7.5% over tuning, to prevent the jumps in the steady-state absorber amplitude as described in chapter two [4]. These absorbers were designed to absorb the second order vibrations that are caused by the firing of the cylinders during four-cylinder mode. In eight-cylinder mode, the two vehicles should perform similarly because the absorbers will be essentially inactive. The experimental results in section 4.2 demonstrate that the CPVA's do indeed effectively absorb the second-order vibrations during operation in four-cylinder mode. The crankshaft used in the experimental engine with CPVA's is shown in Figure 4.1.

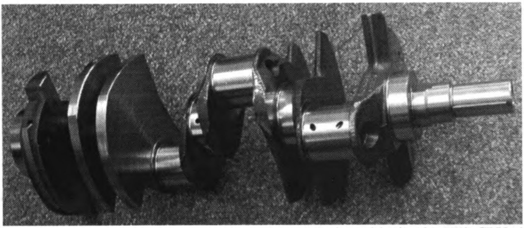

Figure 4.1: Crankshaft used in the experimental engine with circular path CPVA's attached.

The vibration levels at locations selected based on the test procedures provided by Ford Motor Company were measured in both vehicles for a variety of operating conditions [27, 28]. At lower load levels, the pendulums are not as active, so it is expected that the difference in the magnitudes of the second order vibration levels between the vehicle with absorbers and the vehicle without absorbers will not be as pronounced as it is at higher load levels. As the load level increases, the amplitude of the oscillating torque applied to the crankshaft increases, which results in an increase in the pendulums' amplitudes. The increased pendulum amplitude results in an increased torque, with a dominant second-order harmonic component, that cancels all, or part, of the second order component of the oscillating component of the applied torque, thereby reducing the second order vibrations that would have been transmitted to the other vehicle components. By contrast, in the vehicle without absorbers, increases in the amplitude of the second-order component of the applied torque will result in larger forces that will be transmitted to the rest of the vehicle through the motor mounts and the transmission, which will result in larger second-order vibration levels in the vehicle. This behavior will be demonstrated in the experimental results.

4.1 Experimental Results

Using the experimental setup described in appendix two, the acceleration levels at various locations for a variety of operating conditions were measured. The first vehicle tested had the engine with the crankshaft shown in Figure 4.1 that had CPVA's attached to it, and the second vehicle had an identical engine but without the CPVA's. The vehicles were essentially identical in other respects. The accelerometer measurements for the operating conditions listed below demonstrate how the vibration levels in the two test vehicles change for different loads and excitation orders, and thereby illustrate the effectiveness of the CPVA's. The operating conditions were:

1. V4 mode, electrical consumers off, transmission in park (V4-Off-Park).
2. V4 mode, electrical consumers on, transmission in park (V4-On-Park).
3. V4 mode, electrical consumers off, transmission in drive (V4-Off-Drive).
4. V4 mode, electrical consumers on, transmission in drive (V4-On-Drive).
5. V8 mode, electrical consumers off, transmission in park (V8-Off-Park).
6. V8 mode, electrical consumers on, transmission in park (V8-On-Park).
7. V8 mode, electrical consumers off, transmission in drive (V8-Off-Drive).
8. V8 mode, electrical consumers on, transmission in drive (V8-On-Drive).

For both vehicles, and for all the operating cases listed above, the acceleration levels at all measurement positions were recorded over a thirty-second time interval while the engine was idling. In order to examine the effectiveness of the CPVA's in absorbing the second-order torque pulses and reducing the vibration levels in the vehicle, the data was both plotted versus time and converted to the frequency domain using a spectrum averaging routine. The following series of representative plots of the experimental results illustrate the effectiveness of the pendulums in reducing the vibration levels, and more specifically, the second order vibration levels present in the vehicle with absorbers during operation in four-cylinder mode. Figure 4.2, Figure 4.3, Figure 4.4, and Figure 4.6 show the power spectral density of the acceleration measurements versus the engine order, while Figure 4.5 shows a comparison of the signals from an accelerometer at the same position in both vehicles versus time.

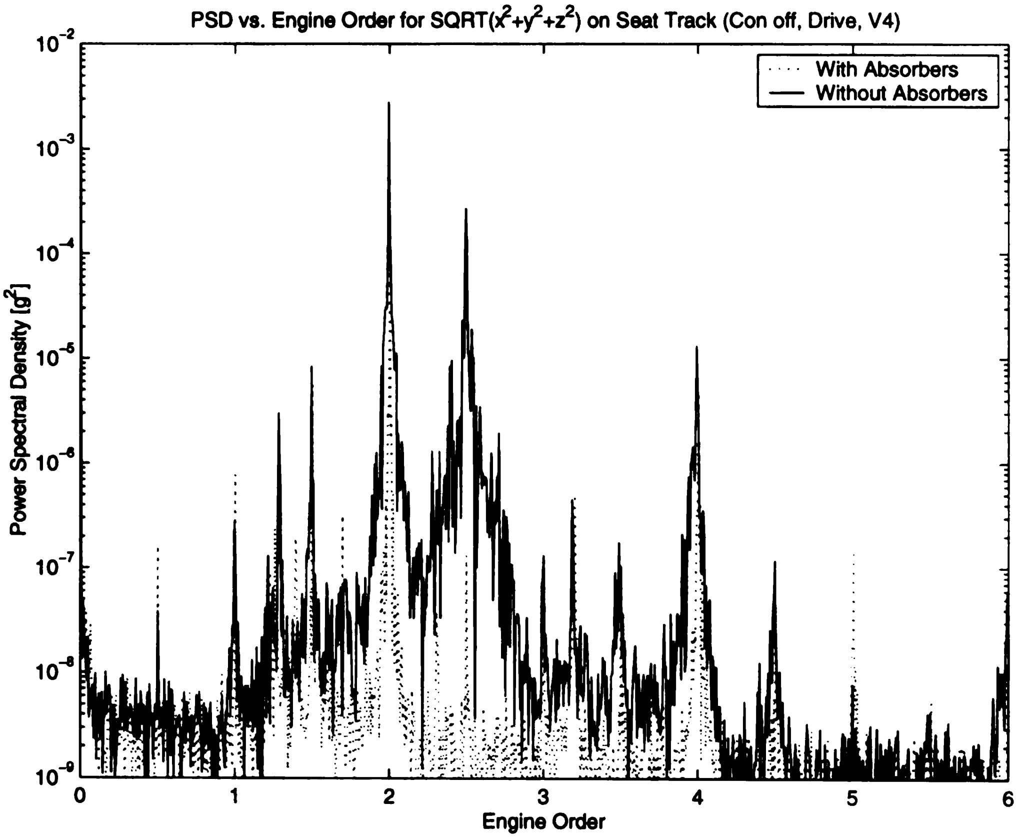

Figure 4.2: Power spectral density of the sum of vibration levels on the seat track versus engine order for the case V4-Off-Drive.

Figure 4.2 illustrates that the overall acceleration levels in the vehicle with the engine with pendulum absorbers are noticeably smaller than the acceleration levels in the vehicle with the engine without pendulum absorbers. In fact, the magnitude of the dominant second order acceleration level measured in the vehicle with absorbers is 75%

smaller than the magnitude of the second order acceleration level measured in the vehicle without absorbers.

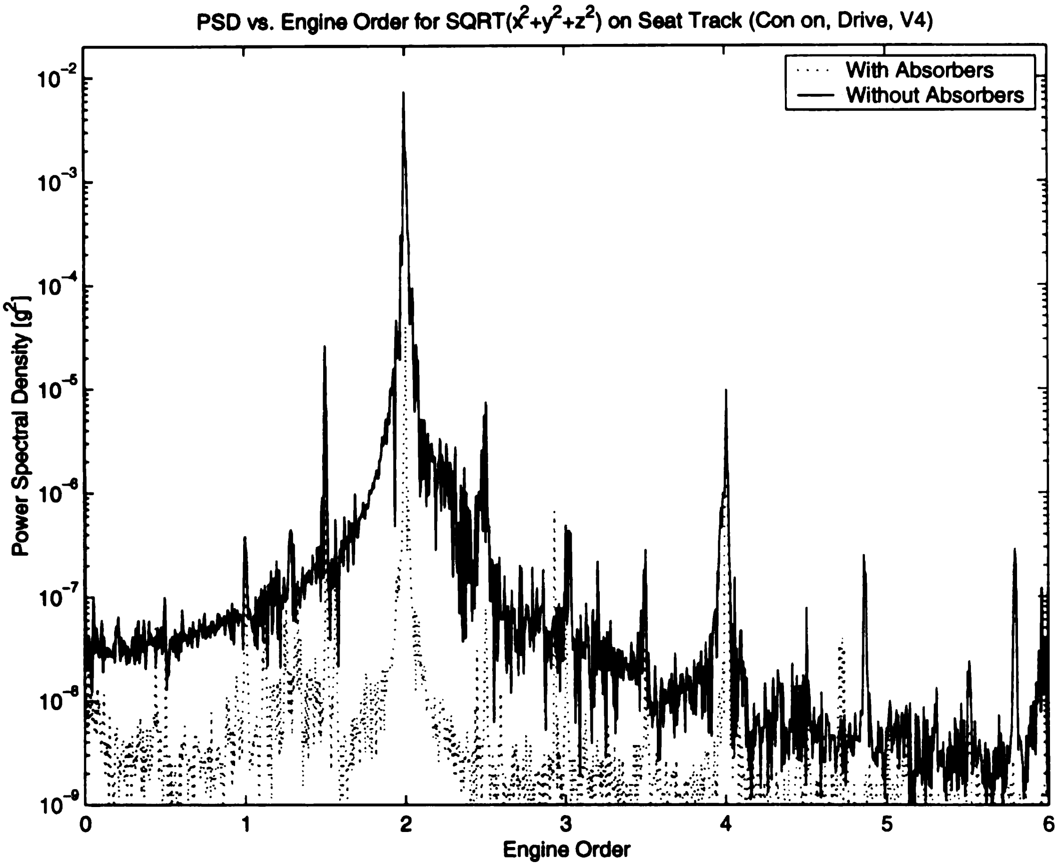

Figure 4.3: Power spectral density of the sum of vibration levels on the seat track versus engine order for the case V4-On-Drive.

Figure 4.3, like Figure 4.2, compares the overall acceleration levels measured on the seat track in the two vehicles, but Figure 4.3 shows the operating condition when the electrical consumers are on in both vehicles while Figure 4.2 showed the results for the operating condition when the electrical consumers in both vehicles are off. The operating condition for Figure 4.3 corresponds to a higher engine load than the operating condition for Figure 4.2. The data plotted in Figure 4.3 and Figure 4.2 definitively shows that the magnitude of the dominant second order vibration in the vehicle with absorbers is significantly lower than the magnitude of the second order vibration in the vehicle without absorbers. In Figure 4.3, the magnitude of the second order vibration in the vehicle with absorbers is only 8% of the magnitude of the second order vibration level in the vehicle without absorbers. Taken together, Figure 4.2 and Figure 4.3 illustrate that the difference in the magnitude of the second order vibration levels in the vehicle with CPVA's and the vehicle without CPVA's becomes more pronounced at higher engine load levels. This agrees with our expectations.

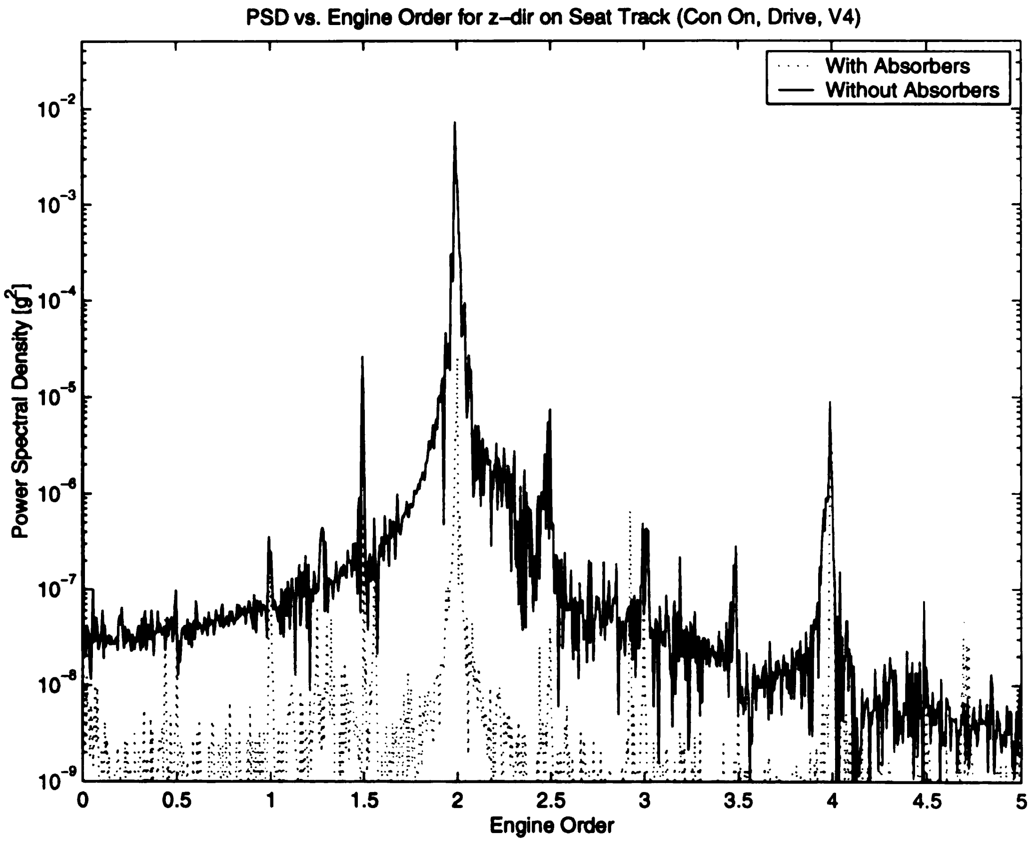

Figure 4.4: Power spectral density of the acceleration levels on the seat track in the z-direction (vertical direction) versus engine order for the case V4-On-Drive.

Figure 4.4 and Figure 4.3 clearly illustrate that the component of the vibration in the z-direction is the dominant directional component of the vibration signal on the seat track. The second-order component of the acceleration signal was the dominant harmonic in Figure 4.2, 4.3, and 4.4. The magnitude of the second order component of the acceleration signal in Figure 4.4 was 94% smaller in the vehicle with absorbers than in the vehicle without absorbers. This plot, like Figures 4.3 and 4.2, clearly demonstrates that second order vibration levels in the vehicle with pendulums are lower than in the vehicle without CPVA's. Figure 4.5 shows the dramatic differences between the measured vibration levels on the seat track in the two vehicles with respect to time. The measurements used to produce Figure 4.5 are the same as those used to produce Figure 4.4, but Figure 4.5 is plotted in the time domain while Figure 4.4 was plotted in the frequency domain.

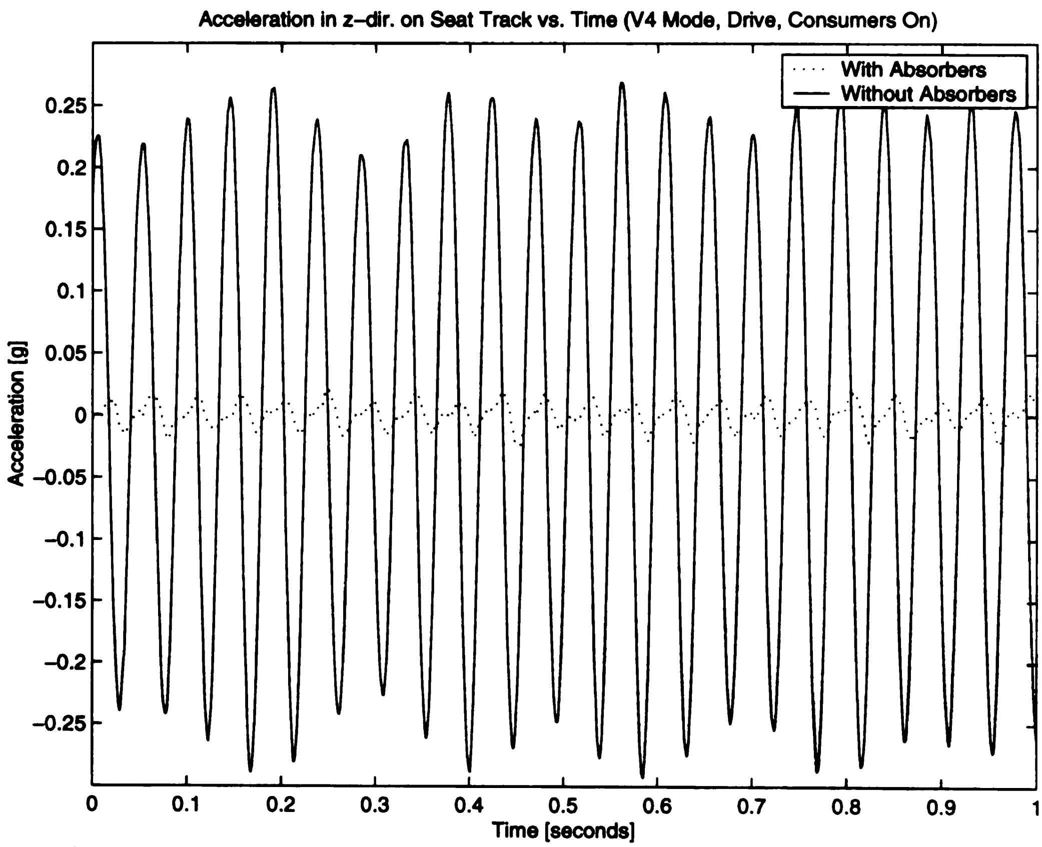

Figure 4.5: Acceleration measurements versus time in the z-direction on the seat track for the case V4-On-Drive.

Figure 4.5 illustrates that the overall vibration level measured in the vehicle with absorbers is much smaller than the vibration level measured in the vehicle without absorbers. The time trace in Figure 4.5 also demonstrates that the vibration signals consist of multiple harmonic components, which were also clearly shown in the spectrum for this data in Figure 4.4. Figure 4.4 and Figure 4.5 both demonstrate that installing absorbers on the crankshaft resulted in a lower magnitude of the overall vibration at this position in the vehicle for the operating condition corresponding to the highest engine load level tested. Figures 4.2-4.5 all focused on the vibration levels measured on the seat track of the two vehicles. Figure 4.6 shows that the absorbers were also effective at reducing the magnitude of the second order vibration on the brake pedal in the same manner that the vibration levels were reduced on the seat track.

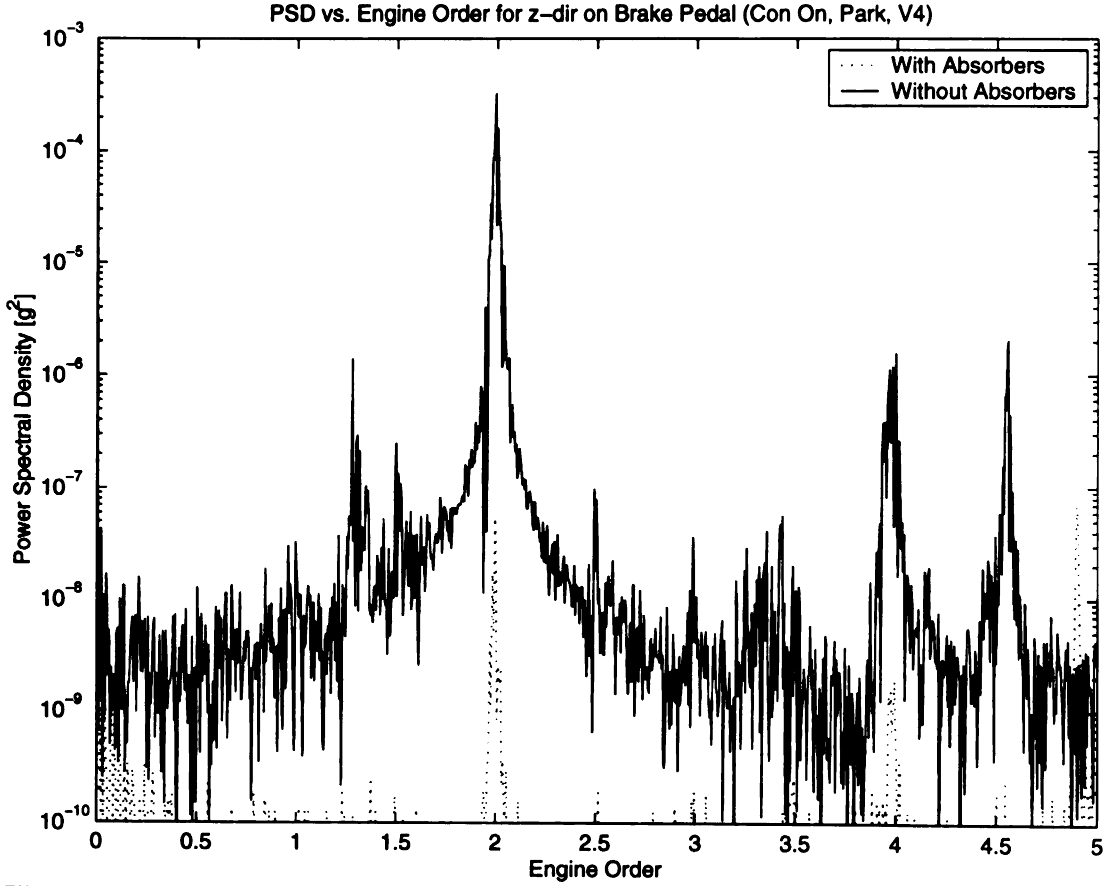

Figure 4.6: Power spectral density of the acceleration levels in the z-direction on the brake pedal (in direction of pedal movement) versus engine order for both vehicles for the case V4-On-Park.

Figure 4.6 possesses many of the same qualitative features that are contained in Figures 4.2-4.4, but Figure 4.6 shows the vibration levels on the brake pedal while Figures 4.2-4.4 all showed the vibration levels measured on the seat track. The magnitude of the second order vibration measured at the brake pedal in the vehicle with absorbers is only 2% of the level in the vehicle without absorbers. Table 4.1 shows a summary of the results for all the operating conditions and all the measurement locations.

Amplitude of Second Order Peak, V4 Mode [g]

		Park, Con Off	Park, Con On	Drive, Con Off	Drive, Con On
Seat Track					
x	with pendulums	6.89E-03	6.19E-03	1.13E-02	3.90E-03
	without	4.28E-03	5.16E-03	1.14E-02	6.51E-03
y	with pendulums	1.34E-02	1.33E-02	2.21E-02	1.14E-02
	without	1.12E-02	1.02E-02	3.72E-03	9.23E-03
z	with pendulums	1.29E-02	1.33E-02	2.21E-02	1.01E-02
	without	2.69E-01	2.08E-01	1.05E-01	1.70E-01
sum	with pendulums	1.58E-02	1.59E-02	2.65E-02	1.29E-02
	without	2.69E-01	2.08E-01	1.05E-01	1.70E-01
Brake z	with pendulums	5.01E-04	4.67E-04	6.41E-04	1.98E-04
	without	5.01E-02	2.26E-02	3.05E-02	4.16E-02
Steering Wheel					
12:00	with pendulums	7.04E-03	6.75E-03	1.25E-02	6.66E-03
	without	4.07E-02	3.17E-02	1.85E-02	4.68E-02
3:00	with pendulums	1.75E-02	1.36E-02	2.00E-02	4.05E-02
	without	1.02E-02	9.10E-03	1.89E-02	1.79E-02
Rear Pinion					
	with pendulums			2.66E-02	2.66E-02
	without			2.11E-02	1.14E-02

Table 4.1: Magnitude of second order component of acceleration of measurements for all operating conditions.

Table 4.1 shows that the magnitudes of the second order vibration signals are not improved for all operating conditions and measurement positions, but for many measurement positions and operating conditions the improvements are dramatic. Table

4.1 shows that the magnitudes of the second order components of the vibration signals were often an order of magnitude lower in the vehicle with absorbers. For the other cases, the magnitudes of the second order component of the vibration signal for both vehicles are at least comparable. Table 4.2 helps to better understand the responses for the few cases when the vehicle with absorber appears to be performing worse in Table 4.1. It shows the ratios of the amplitude of the second order peaks in V4 mode to the amplitude of the second order peaks in V8 mode for both vehicles.

Ratio of Amplitude of Second Order Peak in V4 Mode to V8 Mode

		Park, Con Off	Park, Con On	Drive, Con Off	Drive, Con On
Seat Track					
x	with	22.03	18.34	16.84	6.87
	without	9.16	11.75	18.65	11.58
y	with	24.21	126.68	22.59	60.07
	without	39.84	22.16	10.28	36.10
z	with	10.72	11.92	8.22	7.65
	without	23.47	15.49	36.21	72.73
sum	with	12.96	14.24	9.80	9.67
	without	23.47	15.49	36.19	72.67
Brake z	with	9.34	18.05	10.90	0.15
	without	22.89	9.27	44.58	17.74
Steering Wheel					
12:00	with	28.02	10.39	64.96	11.54
	without	25.61	21.12	6.92	19.54
3:00	with	22.76	5.67	17.57	31.36
	without	38.89	19.67	33.76	37.84
Rear Pinion					
	with			6.77	6.77
	without			28.42	15.30

Table 4.2: Ratio of the magnitude of the second order component of the vibration in V4 mode to the second order component of the vibration signal in V8 mode.

Table 4.2 illustrates clearly how the vibration levels in the vehicles change between eight-cylinder mode and four-cylinder mode. In eight-cylinder mode, the pendulums are inactive, so the two vehicles should have the same dynamic response. Scaling the vehicles' second order components of the vibration in V4 mode by their second order components in V8 mode helps to account for any differences between the vehicles. The above table confirms that for the load cases when the pendulums are less active, the improvement offered by installing CPVA's is not as pronounced as it is when the load is increased. The column on the far right, which corresponds to the largest load level, shows that the vehicle with CPVA's had much less of an increase between V8 mode and V4 mode in the magnitude of the second order component of the vibration signal than the vehicle without absorbers had, with the exception of the y-direction on the seat track where the acceleration levels are small anyway. The measurements in the last row, which were taken directly from the drive shaft's rear pinion, demonstrates how adding absorbers to the vehicle has reduced the vibration levels being transmitted by the engine to the rest of the power train and by extension to the rest of the vehicle.

4.2 Summary of Results for Variable Displacement Internal Combustion Engines

These results illustrate that the vehicle with absorbers had comparatively lower second order vibration levels when operated in V4 mode as shown by the experimental results displayed in Figures 4.4-4.8. The ratios of the second order vibration levels in V4 mode to V8 mode were shown to be much better for the vehicle with absorbers, especially at higher load levels. These results demonstrate the effectiveness of absorbers for eliminating the second order vibrations caused by deactivating four cylinders in an eight-cylinder internal combustion engine. The same results would be expected if three cylinders were deactivated in a six-cylinder engine, or other similar scenarios. The measured vibration levels in the vehicle with absorbers were at or near commercially acceptable levels.

There remain a few measurement locations and directions with results that are contrary to what was expected. No convincing reason for this behavior was discovered during the experiments, but these differences could be caused by truck-to-truck variability in the mode shapes or other small differences in the vehicles tested. The primary purpose of this study was to demonstrate that attaching CPVA's improved the overall vibration levels in a commercial vehicle. The results presents clearly show that this objective has been achieved.

CHAPTER FIVE

SUMMARY AND RECOMMENDATIONS FOR FUTURE WORK

This thesis investigated the behavior and application of circular path centrifugal pendulum vibration absorbers. These CPVA's were shown to reduce torsional vibrations in both controlled laboratory experiments and in an experimental internal combustion engine.

In the laboratory experiments, the results for the case with one active absorber were shown to agree well with both simulations and the theoretical predictions for forcing orders near the absorber's tuning order. However, contrary to expectations from the theory, which is based on asymptotic expansions, the experimental results matched the simulations better as the level of detuning was increased. For all forcing orders considered, the fluctuating torque amplitude at the jump location agreed well with simulations, but both the experiments and the simulations jumped sooner than predicted by the theoretical approximation. Although the experimental torque amplitude agreed well with the simulation torque amplitude at the jump location, the experimental absorber amplitude at the jump location did not agree with the simulations as well as desired. Over a specific operation range, the torsional vibrations were lowered by attaching absorbers to the rotor. The stable upper branch of the solution curve and the hysteresis behavior predicted by the theory were also observed in the single absorber experiments at multiple torque orders. As expected, the absorber amplified rather than absorbed the torque when the response was on the upper branch of the solution curve. This resulted in higher torsional vibrations.

The experimental results for the case with four active absorbers showed even more complex dynamics than anticipated. The expected non-unison responses and bifurcations of unison responses to non-unison responses were observed, but the absorbers did not oscillate in unison at low torques as expected. As the fluctuating torque amplitude was increased, additional absorbers became active and began to move in unison with the previously active absorbers. After all four absorbers were oscillating in unison, the expected bifurcation to non-unison was observed experimentally.

Attaching CPVA's to the crankshaft of a commercial vehicle was shown to improve the vibration levels at various locations throughout the vehicle. Although not all locations were improved, overall, the vibration levels in the vehicle were improved by attaching CPVA's to the crankshaft.

Some suggestions for future work include:

- Investigating the damping mechanism in the absorbers. Linear viscous damping was assumed, but the damping was shown to be a function of the amplitude of oscillation. This could be the cause of the discrepancy between the experimental absorber amplitude and the simulation absorber amplitude.
- Analytically investigate the non-unison absorber response at low torques. Specifically, the activation of additional absorbers as the torque amplitude is increased is currently not well understood.

- Measure the vibration levels in the experimental vehicles after redesigning the crankshaft so that the engine can be operated using the same crankshaft with the absorbers either locked or unlocked. This will eliminate any the truck-to-truck variability.
- Repeat the experiments reported in Chapter Three for other absorber paths including cycloidal paths, epicycloidal paths, and subharmonic epicycloidal paths.
- Investigate the absorber response to multi-harmonic torques.

APPENDICES

APPENDIX ONE

EXPERIMENTAL ABSORBER DAMPING MEASUREMENT

To measure the damping levels experimentally, three of the four absorbers were locked. With one absorber free and the rotor spinning at a known mean speed, a fluctuating torque was applied to the rotor. Once the absorber had reached steady state, the fluctuating torque was turned off and the absorber response was measured, as shown in Figure A1.1 for absorber four. The absorber damping ratio was approximated using the log decrement method, which is given by:

$$\zeta = \frac{\ln\left(\frac{x_0}{x_n}\right)}{2\pi n} \tag{A1.1}$$

for small damping, where x_0 is the amplitude of the first response peak, x_n is the amplitude of the n^{th} response peak, and ζ is the damping ratio. For example, selecting two peaks in the larger amplitude response range for the measurement data shown in Figure A1.1:

$x_0 = 13.5^\circ$
$x_4 = 6.0^\circ$

Using these measurements, $\zeta = 0.0323$. This process was repeated for all four absorbers.

The absorber damping values were found to vary cubicly with the absorber amplitude. In order to match the experimental and simulation responses as well as possible near the jump, the viscous damping ratio as calculated at large amplitudes was used for all calculations.

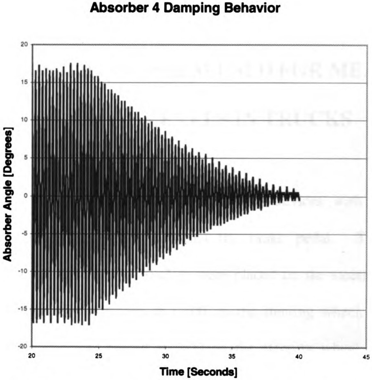

Figure A1.1: Absorber amplitude versus time for absorber four.

APPENDIX TWO

DATA ACQUISITION SYSTEM USED FOR MEASURING VIBRATION LEVELS IN TRUCKS

Tri-axial accelerometers produced by Analog Devices with sensitivities of 500mV/g were used on the seat track and the brake pedal. Two single axis accelerometers with sensitivities of 10mV/g were placed on the steering wheel. One single axis accelerometer was placed at 12:00 on the steering wheel, and the second single axis accelerometer was placed at 3:00 on the steering wheel. Both of these accelerometers were placed to measure vibrations in the plane of the steering wheel. The accelerometer locations are shown in figures A2.2, A2.3, A2.4, and A2.5. On the brake pedal, the z direction measures the vibrations in the direction of the pedal movement. For the seat track accelerometer, the x-direction is parallel to the seat track, the y-direction is perpendicular to the seat track, and the z-direction is the positive vertical direction.

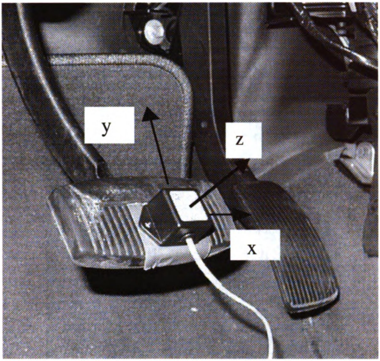

Figure A2.2: Accelerometer position on brake pedal.

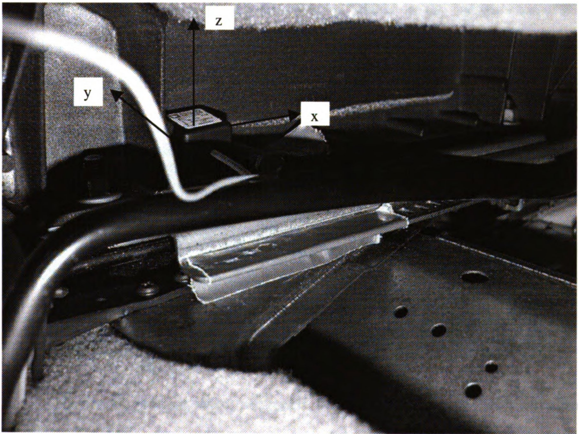

Figure A2.3: Accelerometer position on seat track.

Figure A2.4: Accelerometer positions on steering wheel.

In addition to the accelerometer positions shown in the figures above, the vibration levels were also recorded at the pinion, shown in Figure A2.5, for the cases when the transmission was in drive and the consumers were both on and off.

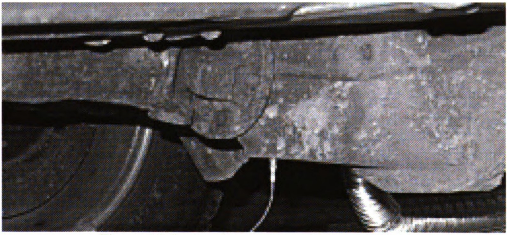

Figure A2.5: Accelerometer position on pinion.

The accelerometers were connected to an eight channel GX-1 recorder manufactured by TEAC. The seat track, brake pedal, and steering wheel vibration levels were recorded simultaneously. The vibration levels at the pinion were recorded during a separate experimental run. Measurements were taken for 30 seconds for each operating case at a sampling rate of 1000 Hz. The data was recorded on a laptop computer for all operating cases.

BIBLIOGRAPHY

BIBLIOGRAPHY

[1] B.C. Carter, *British Patent No. 337, 446*, 1929.

[2] V. Moore. The control of torsional vibration in radial aircraft engines by means of tuned pendulums. *Journal of Aeronautical Science*, 9:229-244, 1942.

[3] W. Ker Wilson. *Practical Solution of Torsional Vibration Problems*, chapter XXX. Volume IV, Chapman and Hall Ltd, London, 3rd edition, 1968.

[4] D. E. Newland. Nonlinear aspects of the performance of centrifugal pendulum vibration absorbers. ASME Journal of Engineering for Industry, 86:257-263.

[5] M. Cook. Absolute absorption. *Car Craft*, August 1994: 75.

[6] J. F. Madden. Constant frequency bifilar vibration absorber. *United States Patent No. 4218187*, 1980.

[7] V. K. Garg. *Effects of Mistuning on the Performance of Centrifugal Pendulum Vibration Absorbers*. MS thesis, Michigan State University, 1996.

[8] C-T. Lee and S. W. Shaw. A comparative study of nonlinear centrifugal pendulum bibration absorbers. *Journal of Sound and Vibration*, 203(5): 731-743, 1997.

[9] M. Sharif-Bakhtiar and S. W. Shaw. Effects of nonlinearities and damping on the dynamic response of a centrifugal pendulum absorber. *ASME Journal of Vibration and Acoustics*, 114:305-311, 1992.

[10] A. S. Alsuwaiyan and S. W. Shaw. Localization in systems of nearly-identical torsional vibration absorbers. *Proceedings of the Workshop on Vibration in Rotating Machinery held at King Fahd University Department of Petroleum & Minerals, Dhahran, Saudi Arabia, April 29-May 1, 2000*, pages 205-216. King Fahd University of Petroleum & Minerals Printing Press, 2001.

[11] A. S. Alsuwaiyan. *Performance Stability and Localization of Systems of Vibration Absorbers*. PhD Thesis, Michigan State University, 1999.

[12] C. F. Taylor. *The Internal-Combustion Engine in Theory and Practice*, volume 2, chapter 8. The M. I. T. Press, Cambridge, Massachusetts, revised edition, 1985.

[13] O'Connor. The viscous torsional vibration damper. *Society of Automotive Engineering Quarterly Transactions,* 1:87, 1947.

[14] Pierce. Rubber mounted dampers, examples of application. *Transactions of Society of Automotive Engineering*, 53: 480, 1945.

[15] C-T. Lee, S. W. Shaw, and V. T. Coppola. A subharmonic vibration absorber for rotating machinery. *ASME Journal of Vibration and Acoustics*, 119: 590-595, 1997.

[16] J. P. Den Hartog. *Mechanical Vibrations*. Dover Publications, Inc. New York. 1985.

[17] C-P. Chao. *The Performance of Multiple Pendulum Vibration Absorbers Applied to Rotating Systems*. PhD Thesis, Michigan State University, 1997.

[18] M. H. Hamouda and G.A. Pierce. Helicopter vibration suppression using simple pendulum absorbers on the rotor blade. *Journal of American Helicopter Society*, 29(3): 19-29, July 1984.

[19] W. Miao and T. Mouzakis. Nonlinear characteristics of the rotor bifilar absorber. *37th American Helicopter Society Forum*, 1981.

[20] V. J. Borowski, H. H. Denman, D. L. Cronin, S. W. Shaw, J. P. Hanisko, L. T. Brooks, D. A. Milulec, W. B. Crum, and M. P. Anderson. Reducing vibration of reciprocating engines with crankshaft pendulum vibration absorbers. 1991. SAE Technical Paper Series 911876.

[21] D. L. Cronin. Shake reduction in an automobile engine by means of crankshaft-mounted pendulums. *Mechanism and Machine Theory*, 27(5):517-533, 1992.

[22] H. H. Denman. Tautochronic bifilar pendulum torsion absorbers for reciprocating engines. *Journal of Sound and Vibration*, 159:251-277, 1992.

[23] S. W. Shaw, V. K. Garg, and C-P. Chao. Attenuation of engine torsional vibrations using tuned pendulum absorbers. Volume 2, pages 713-722. *The Society of Automotive Engineers, 1997. SAE Noise and Vibration Conference and Exposition.*

[24] M. A. Wachs. The main rotor bifilar absorber and its effect on helicopter reliability/maintainability. 1973. SAE Technical Paper Series 730894.

[25] A. G. Haddow and S. W. Shaw. An experimental study of torsional vibration absorbers. *Proceedings of Design Engineering Technical Conference 2001, Pittsburgh, PA, September 9-12.*

[26] C-P. Chao, S.W. Shaw, and C-T. Lee. Non-unison dynamics of multiple centrifugal pendulum vibration absorbers. Journal of Sound and Vibration, 204(5): 769-794, 1997.

[27] Ford Motor Company. Vehicle NVH test procedure (VNVHTP #28), Vehicle operation-idle sweep. *Corporate Engineering Test Procedure*. 00.00-R-492.

[28] Ford Motor Company. Idle/NVH quality operating measurement procedure. *Corporate Engineering Test Procedure*. 00.00-L-403.